

## Article

# Novel Hominid-Specific IAPP Isoforms: Potential Biomarkers of Early Alzheimer's Disease and Inhibitors of Amyloid Formation

Qing-Rong Liu \*, Min Zhu, Qinghua Chen , Maja Mustapic , Dimitrios Kapogiannis  and Josephine M. Egan \*

Laboratory of Clinical Investigation, NIA-NIH, 251 Bayview Blvd, Baltimore, MD 21224, USA

\* Correspondence: qliu@mail.nih.gov (Q.-R.L.); eganj@grc.nia.nih.gov (J.M.E.)

**Abstract:** (1) Background and aims: Amyloidosis due to aggregation of amyloid- $\beta$  ( $A\beta_{42}$ ) is a key pathogenic event in Alzheimer's disease (AD), whereas aggregation of mature islet amyloid polypeptide (IAPP<sub>37</sub>) in human islets leads to  $\beta$ -cell dysfunction. The aim of this study is to uncover potential biomarkers that might additionally point to therapy for early AD patients. (2) Methods: We used bioinformatic approach to uncover novel IAPP isoforms and developed a quantitative selective reaction monitoring (SRM) proteomic assay to measure their peptide levels in human plasma and CSF from individuals with early AD and controls, as well as postmortem cerebrum of clinical confirmed AD and controls. We used Thioflavin T amyloid reporter assay to measure the IAPP isoform fibrillation propensity and anti-amyloid potential against aggregation of  $A\beta_{42}$  and IAPP<sub>37</sub>. (3) Results: We uncovered hominid-specific IAPP isoforms: hIAPP $\beta$ , which encodes an elongated propeptide, and hIAPP $\gamma$ , which is processed to mature IAPP<sub>25</sub> instead of IAPP<sub>37</sub>. We found that hIAPP $\beta$  was significantly reduced in the plasma of AD patients with the accuracy of 89%. We uncovered that IAPP<sub>25</sub> and a GDNF derived DNSP<sub>11</sub> were nonaggregating peptides that inhibited the aggregation of IAPP<sub>37</sub> and  $A\beta_{42}$ . (4) Conclusions: The novel peptides derived from hIAPP isoforms have potential to serve as blood-derived biomarkers for early AD and be developed as peptide based anti-amyloid medicine.



**Citation:** Liu, Q.-R.; Zhu, M.; Chen, Q.; Mustapic, M.; Kapogiannis, D.; Egan, J.M. Novel Hominid-Specific IAPP Isoforms: Potential Biomarkers of Early Alzheimer's Disease and Inhibitors of Amyloid Formation. *Biomolecules* **2023**, *13*, 167. <https://doi.org/10.3390/biom13010167>

Academic Editors: Alexei Finkelstein and Maria Gasset

Received: 18 November 2022

Revised: 23 December 2022

Accepted: 9 January 2023

Published: 13 January 2023



**Copyright:** © 2023 by the authors. Licensee MDPI, Basel, Switzerland. This article is an open access article distributed under the terms and conditions of the Creative Commons Attribution (CC BY) license (<https://creativecommons.org/licenses/by/4.0/>).

**Keywords:** amyloids; Alzheimer's disease; diabetes; biomarkers; evolution; alternative splicing

## 1. Introduction

Human islet amyloid polypeptide (IAPP), a member of the calcitonin-like gene family, is co-released with insulin from pancreatic  $\beta$ -cells upon glucose stimulation. It forms toxic  $\beta$ -sheets, oligomers, and fibrils in cytoplasm and around  $\beta$ -cells, thereby contributing to  $\beta$ -cell dysfunction [1,2]. The amyloidogenic propensity of primate IAPP is an evolutionary conundrum, since IAPP does not form fibrils in some mammalian species that lack the core amyloid sequences, while it does so in other species [3]. The quantity of macromolecules involved in various proteostasis mechanisms (i.e., control of membrane IAPP trafficking, proteasome degradation, endoplasmic reticulum unfolded protein response (UPR), and autophagy) [4] are drastically reduced in  $\beta$ -cells compared to other islet cell types [5], since insulin and IAPP account for more than one-half of their mRNA and protein content [6,7]. Therefore, human evolution adaptation may have led to additional intra- and extracellular chaperones to counter the proteinopathies of  $\beta$ -cells. Proinsulin and insulin are known inhibitors of IAPP aggregation [8], and we recently found that a short 19-AA C $\alpha$ -peptide derived from the 74-AA proinsulin isoform inhibited fibrillation of IAPP<sub>37</sub> [9]. In this investigation, we report additional peptide chaperones, a nonaggregating IAPP<sub>25</sub> from  $\beta$ -cells, and a DNSP<sub>11</sub> from  $\alpha$ -cells that inhibit fibrillation of human mature IAPP<sub>37</sub> and  $A\beta_{42}$ .

Human 89-AA proIAPP undergoes extensive posttranslational modification: cleavage of a 22-AA signal peptide and formation of a disulfide bond between Cys-2 and -7 in the endoplasmic reticulum resulting in 67-AA proIAPP that is transported to the Golgi

apparatus and then packaged in secretory granules (SG); it is further processed, similar to proinsulin processing, to remove an 11-AA proIAPP<sub>11</sub> peptide from the N-terminus by prohormone convertase 2 (PC2) and a 16-AA peptide from the C-terminus by PC1/3 [10]. The Lys-Arg AAs at the C-terminus are then removed by carboxypeptidase E, and peptidyl-glycine  $\alpha$ -amidating monooxygenase (PAM) amidates the remaining glycine that is then converted to an amide group at the C-terminus of IAPP<sub>37</sub> and release of glyoxylate [11]. The resulting mature IAPP<sub>37</sub> is primarily localized in the halo of secretory granules (SG) (the pale outer area of  $\beta$ -cell SG seen on electron microscopic images) alongside C-peptide, while insulin itself is in the dense core of SG in  $\beta$ -cells [12].

We hypothesized that chaperones secreted from healthy  $\alpha$ - and  $\beta$ -cells could counter IAPP<sub>37</sub> aggregation in human islets. Glial cell-derived neurotrophic factor (GDNF), which is protective to dopaminergic neurons [13], is enriched in pancreatic islets [14] and is actually expressed at higher levels in the islets than in the brain [15]. Mwangi et al. found that GDNF can enhance  $\beta$ -cell proliferation and mass [16,17], whereas Lucini et al. found that GDNF colocalized only with glucagon-expressing  $\alpha$ -cells in the pancreas [18]. The pro-peptide of a longer GDNF $\alpha$  isoform is cleaved by prohormone convertases to produce an amidated dopamine neuron stimulating peptide containing 11-AA (DNSP<sub>11</sub>; PPEAPAEDRSL) that is protective to dopaminergic neurons in animal models of Parkinson's disease [19–21]. However, there is no report of DNSP<sub>11</sub> inhibiting IAPP<sub>37</sub> aggregation. Therefore, we carried out a ThT amyloid inhibitory assay with the novel hIAPP<sub>25</sub> and the known DNSP<sub>11</sub> in this study.

The common feature of T2DM and AD is progressive self-aggregation of an amyloidogenic protein, predominantly IAPP<sub>37</sub> in islets and A $\beta$  in brain regions. However, IAPP<sub>37</sub> fibrils also deposit in cerebral vessels [22] and cross-seed with A $\beta$  during the formation of amyloid plaques [23,24]. Also pointing to a relationship between AD and T2DM, plasma IAPP (and insulin) levels are reduced in mild cognitive impairment (MCI) and AD patients [25,26] and in the later stages of T2DM [27]. A nonaggregating synthetic IAPP, pramlintide, is reported to improve cognition in AD patients and reduce A $\beta$  and phospho-Tau load in the cortex and hippocampus of 5XFAD transgenic mice [28,29]. Flavonoid silybins also inhibit aggregation of both IAPP and A $\beta$  [30,31]. The evidence reinforces the notion that an association between AD and T2DM may rely on the cross-seeding properties of IAPP<sub>37</sub> and A $\beta$  [32,33]. In the present study, using a quantitative SRM proteomic assay, we identified and quantified the translated protein levels of two novel IAPP isoforms: hIAPP $\beta$ , which was increased in the cerebrum and reduced in the plasma of AD patients, and hIAPP $\gamma$ , which encodes a novel mature IAPP that is 25-AA in length, is nonamyloidogenic, and was found to be reduced in T2DM islets and in the plasma of AD patients.

## 2. Materials and Methods

### 2.1. Source of Tissue Samples

Islets from human nondiabetic and T2DM postmortem pancreata [9] were provided by the NIDDK-funded Integrated Islet Distribution Program (IIDP) at City of Hope, NIH Grant # 2UC4DK098085 (<https://iidp.coh.org/> (accessed on 13 July 2017, to 8 April 2019)). A total of 1000–2000 islets were received for each sample, and approximately 200 islets were handpicked for proteomics and the rest for gene expression experiments [9]. Human tissue total RNA was obtained from TaKaRa Bio (Takara Bio USA, San Jose, CA, USA). Plasma and cerebrospinal fluid (CSF) samples were from the IRB-approved study of NCT01255163 (<https://clinicaltrials.gov/ct2/show/NCT01255163> (accessed on 18 November 2016)) [34].

### 2.2. Participants

We tested the diagnostic performance of the SRM assay for hIAPP $\beta$  and hIAPP $\gamma$  in a cohort of 10 individuals with high-probability early AD according to the NIA-AA and IWG-2 criteria [35] and 19 cognitively normal healthy controls. Individuals with AD had abnormal CSF levels of amyloid  $\beta$ -peptide (A $\beta$ ) 1–42 (A $\beta$ <sub>42</sub>) < 192 pg/mL and of P-T181-

$\tau > 23$  pg/mL that supported their high-probability diagnosis [36]. All participants were evaluated at the Clinical Research Unit of the U.S. National Institute on Aging (NIA; Baltimore, MD, USA) under NIH IRP approved protocols.

### 2.3. Bioinformatics and Sanger Sequencing

We used Sequencher 5.4.6 software (Gene Codes Corporation, Ann Arbor, MI, USA) to assemble pancreatic islet and insulinoma EST sequences (<http://www.ncbi.nlm.nih.gov/dbEST/> (accessed on 24 July 2017)) that are homologous to the human *IAPP* gene. IAPP sequences from different species were downloaded from Ensembl (<https://useast.ensembl.org/index.html> (accessed on 26 July 2017)) and UCSC (<https://genome.ucsc.edu/> (accessed on 26 July 2017)) genome browsers. The ExpASY server was used to analyze peptide properties [37], and EMBL-EBI (<https://www.ebi.ac.uk> (accessed on 26 July 2017)) was used for protein sequence alignments. The IMAGE EST clones IMAG6132753, IMAG6028075, and IMAG6218226 were ordered from Source Bioscience (<https://www.sourcebioscience.com/> (accessed on 16 October 2017)), and the inserts were sequenced bidirectionally by the Sanger sequencing service of Eurofins Genomics (Louisville, KY, USA).

### 2.4. RNA Isolation, cDNA Synthesis, RT-qPCR, and ELISA

RNA isolation, cDNA synthesis, and RT-qPCR procedures were described previously [38]. We designed splicing junction specific TaqMan probes (Table S1) for IAPP isoforms that were custom made by Thermo Fisher Scientific (Waltham, MA, USA). The duplex fluorescent TaqMan assay was performed in replicates (StepOnePlus™ real-time PCR system), and the relative fold change was calculated using the Formula  $(2)^{-\Delta\Delta Ct}$  normalized to GAPDH (vic-labeled, Cat# 4326317E) [39]. Droplet digital PCR (ddPCR) absolute values were derived from the Poisson distribution of positive and negative droplets (QX200 ddPCR System (Bio-Rad, Philadelphia, PA, USA), and fam-IAPP isoform-specific droplets were normalized with those of vic-GAPDH. We used 16 AD and 16 non-AD MTG samples and 8 T2DM (fresh) and 15 normal control (13 fresh and 2 frozen) islet samples for ddPCR assay. Plasma IAPP was quantified using a Human IAPP ELISA Kit (Cat# LS-F9686, LSBio, Seattle, WA, USA).

### 2.5. Selected Reaction Monitoring (SRM)-MS Assay

The selected peptides (Table S2) were synthesized as synthetic steady-isotope-labeled (heavy) standard peptide analogs and unlabeled analogs (light) by Genemed Synthesis Inc. (San Antonio, TX, USA). Details of SRM parameters, linear range of quantification, and limit of quantification (LOQ) followed our previous protocol [9]. All sample data generated from the islet (freshly handpicked ~200 islets per donor of T2DM 8 individual donors and control 8 individual donors; 1 in T2DM and 3 in control islet samples did not have SRM data), brain middle temporal gyrus (MTG) (250  $\mu$ g), plasma (5  $\mu$ L), and CSF (250  $\mu$ L) samples were collected using Analyst software version 1.6.3 and processed using MultiQuant software (Sciex, version 3.02 with Scheduled-MRM-Algorithm). Each peak area was manually inspected to ensure correct peak detection and accurate integration. The relative quantitation value of each given peptide was obtained by summing all peak area ratios of the light per heavy from all target transitions of this peptide and then averaging over three technical runs.

### 2.6. Thioflavin T In Vitro Assay for IAPP and A $\beta$ Amyloid Formation

Thioflavin T (ThT) was purchased from Millipore-Sigma (Cat# T3516, Rockville, MD, USA). The APP<sub>37</sub> peptide (37-AA) (Cat# AS-60254-1, amidated C-terminal, and disulfide bridge between Cys2 and Cys7), A $\beta$ <sub>42</sub> (1–42) (Cat# AS-20276), and C-peptide (Cat# AS-61127) were from AnaSpec (Fremont, CA, USA). Black 96-well microplates (Chimney Well) were obtained from Greiner Bio-One (Frickenhausen, Germany). C-terminal amidated IAPP<sub>25</sub>, DNSP<sub>11</sub>, C $\alpha$  (EAEDLQGSLSLQPLALEGSLQ), and INSU (MGSETIKPA-GAQQPSALQDRLHQKRPSSRSLSFCHGVPDAPPAPAGAAGPLGT) derived from human

INS upstream open reading frame peptides [9] were synthesized by GeneMed Synthesis Inc. (San Antonio, TX, USA). Monomeric IAPP<sub>37</sub> and A $\beta$ <sub>42</sub> were made in hexafluoroisopropanol (HFIP, Cat# 105228, Sigma-Aldrich, St. Louis, MO, USA) solution and then lyophilized. The final concentration of the monomeric peptides was 1% DMSO and 25  $\mu$ M ThT in Component A buffer (AnaSpec Manual of SensoLyte Thioflavin T Aggregation Kit, Cat# AS-72214). ThT buffer was used as a blank, and 50  $\mu$ M IAPP<sub>37</sub> or A $\beta$ <sub>42</sub> without inhibitors was used as a control. The final concentrations of IAPP<sub>37</sub> and A $\beta$ <sub>42</sub> with the inhibitory IAPP<sub>25</sub>, DNSP<sub>11</sub>, C $\alpha$ , and INSU peptides were 50  $\mu$ M in the fibrillation kinetic assays [9]. Aggregation was measured by increasing the ThT fluorescent intensity ( $\lambda_{\text{ex}} = 440$  nm,  $\lambda_{\text{em}} = 485$  nm, height 3 mm, flashes 12) for 36 cycles for IAPP<sub>37</sub> and A $\beta$ <sub>42</sub>, 5 min per cycle at 37 °C with 15 s of shaking (100 rpm) between the reads in an EnSpire Multimode Plate Reader (PerkinElmer Inc., Waltham, MA, USA).

### 2.7. Statistical Data Analysis

GraphPad Prism v9 software was used for statistical analysis of RT-qPCR and SRM data.  $p < 0.05$  was considered significant, and data are represented as the means  $\pm$  SEM. The normalized expression values of hIAPP isoforms in TaqMan fold changes and ddPCR IAPP/GAPDH droplets, ELISA, and SRM quantitative values were analyzed with unpaired Student's *t*-test and the Pearson correlation coefficient matrix. Biomarker accuracies were calculated by the area under the receiver operating characteristic curve (AUROC). For the ThT amyloid dye assay, the area under the curve (AUC) was calculated using the trapezoidal rule [40], and the data were analyzed using one-way ANOVA with Tukey's multiple comparisons [41].

## 3. Results

### 3.1. Novel Hominid-Specific Peptides Derived from hIAPP Isoforms as Potential Diagnostic and Therapeutic Targets for AD and T2DM

#### 3.1.1. Identification of hIAPP $\beta$ and hIAPP $\gamma$ Isoforms

We searched dbEST sequences [42] and found 336 ESTs that were homologous to human IAPP mRNA (NM\_000415). Assembly of the ESTs revealed additional protein coding IAPP isoforms of four exons instead of the conventional three exons [43]. We uncovered novel IAPP isoforms composed of four exons (Figure 1A): hIAPP $\beta$  contains an alternatively spliced exon 5 translated into a longer prohormone adding 14-AA to prototype proIAPP<sub>11</sub> of hIAPP $\alpha$ , while hIAPP $\gamma$  contains an alternatively spliced exon 4 translated into an unrelated proIAPP<sub>32</sub> (only 4-AA at the N-terminus conserved to proIAPP<sub>11</sub> of hIAPP $\alpha$ ) and a frameshifted IAPP<sub>25</sub> completely different from IAPP<sub>37</sub> (Figure 1B). The coding sequences (CDSs) of orthologs of novel IAPP exon 4 were only found in hominid (Figure 1C), except for the gibbon ortholog that contains a single nucleotide deletion (Figure S1A), and the orthologs of other primate species contain nucleotide insertions causing frameshifts (Figure S1B). There is one nonsynonymous substitution (Trp/Cys) between human and chimp, indicating adaptive evolution (positive selection) of hIAPP $\gamma$ . The CDS of orthologs of exon 5 was found in hominid and not in old-world monkeys, except for a single nucleotide deletion in *Chlorocebus sabaues* and orthologs of lemurs and marmoset, two small primates evolving separately in Madagascar and South America. There are no nonsynonymous or synonymous substitutions of exon 5 among humans, chimp, and gorillas (Figure S1C), indicating neutral selection of hIAPP $\beta$  in humans. The sequences of all hIAPP coding exons are identical to those of the Neanderthal genome [44].

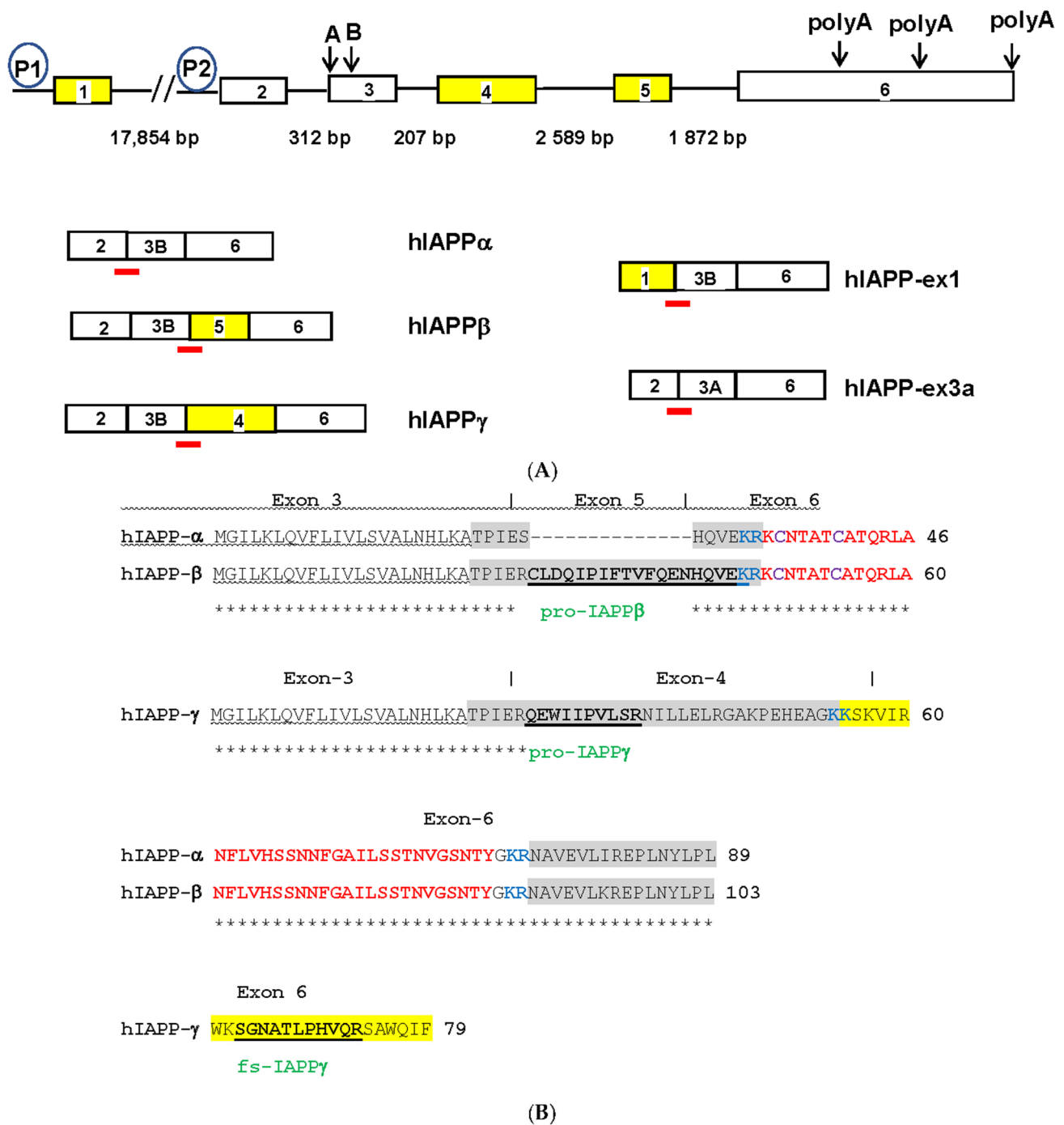
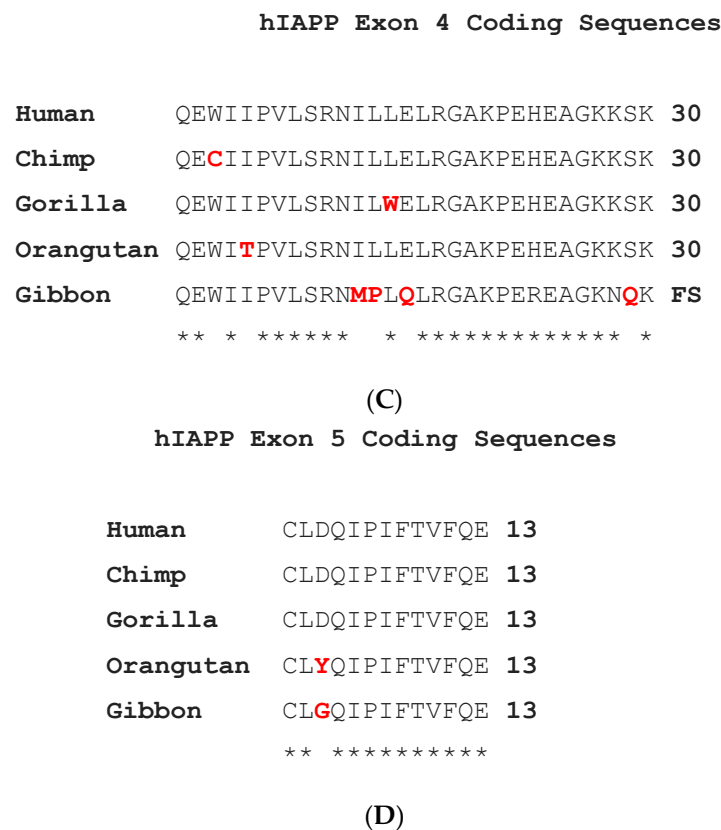


Figure 1. Cont.



**Figure 1.** (A) Human *IAPP* gene structures and alternatively spliced isoforms. Open boxes represent exons, solid lines represent introns of different sizes in base pairs (bp) and P1 and P2 in circles are alternative promoters. Yellow boxes represent hominid-specific *IAPP* exons. Downward arrows and capital letters are at the intra-exonal splicing donor sites in exon 3 and alternative polyadenylation sites in exon 6. The red bars are exon junctional TaqMan probes that hybridize specifically to various *IAPP* isoforms. The spliced transcripts of hIAPP isoforms are named and below the gene structure. hIAPP-ex1 and -ex3a are not expressed and are expressed at low levels in islets, respectively. (B) Alignment of hIAPP $\alpha$ , hIAPP $\beta$ , and hIAPP $\gamma$  amino acid sequences. Homologous amino acids are marked by asterisks, signal peptide underlined by wavy lines, prohormone regions by gray highlight, the convertase dibasic amino acids by blue lettering, mature IAPP<sub>37</sub> by red lettering, bisulfide bond cysteine (C) by purple lettering, IAPP<sub>25</sub> by yellow highlight, the proteolytic peptide names by green lettering, and the sequences are bolded and underlined. Exon numbers are above the sequences and demarcated by the | sign. (C) Alignment of exon 4 of the hIAPP $\gamma$  CDS. (D) Alignment of exon 5 of the hIAPP $\beta$  CDS. The amino acids coded by nonsynonymous substitutions are shown in red lettering.

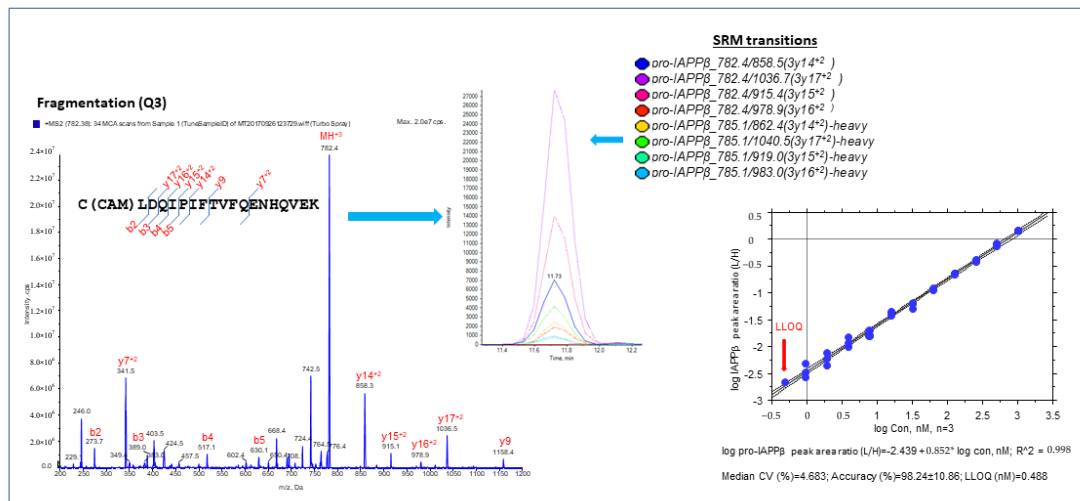
hIAPP $\gamma$  does not contain the C-terminal prohormone region of hIAPP $\alpha$  and is processed to a 25-AA peptide, IAPP<sub>25</sub>, by prohormone convertase (at paired basic amino acid KK in Figure 1B). IAPP<sub>25</sub> (KSKVIRWKSGNATLPHVQRSWQIF) does not contain any amyloid core sequences or consensus sites for proteases at the C-terminus [45], nor does it have any homology with any protein domains, families, or functional sites in the PROSITE database (<https://prosite.expasy.org/> (accessed on 31 January 2018)). It has a theoretical molecular weight (MW) of 2938 Daltons (Dal) and an isoelectric point (pI) of 12.0, which is more basic than IAPP<sub>37</sub> (MW = 3906 Dal, pI = 8.9). We revised the human *IAPP* genomic structure to six exons, of which exon 6 is a constitute exon with three alternative polyadenylation sites at its 3'UTR. Exon 1 (NM\_001329201) and exon 2 are alternative promoter initiation exons, and exon 3 has two intra-exonal splicing sites, including the exon 3A (IAPP-ex3A, BM876150) splicing site 20 bp upstream of conventional exon 3B. IAPP-ex3A isoform expression was approximately 20-fold lower than hIAPP $\alpha$  and hIAPP $\gamma$

(exon 3B splicing site) expression in islets. IAPP-ex1 was conserved only in human, chimp, and gorilla (Figure S1D) and could be detected in testes instead of islets (Figure S2A). To validate the novel IAPP isoforms, we sequenced EST clones of IMAG6132753 (CA771728) and IMAG6028075 (BQ548915) and found that they were full-length cDNA clones of hIAPP $\alpha$  and hIAPP $\gamma$ , respectively. The EST clone IMAG6218226 of hIAPP $\beta$  (CA774544) is not commercially available, so we used mass spectrometry (MS)-based SRM to validate it at the protein level.

### 3.1.2. Validation and Quantification of hIAPP $\beta$ and hIAPP $\gamma$ by MS-Based SRM Assay

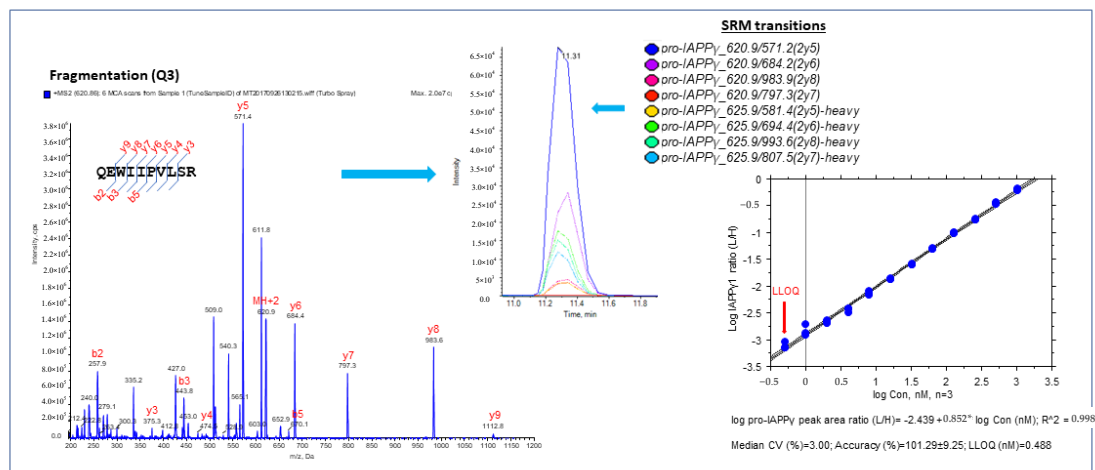
We selected proteotypic peptides based on the empirical procedure that balances ideal attributes of the assays with practical limitations, e.g., hominid-specific CDS of the exon 5 region (pro-IAPP $\beta$ ) and the CDS of exon 4 region (pro-IAPP $\gamma$ ) and the frameshifted (fs) mature peptide region (fs-IAPP $\gamma$ ) (Figure 1B). Interference-free precursors and fragments (transitions) for target proteins constitute the final SRM assay, i.e., four transition pairs for pro-IAPP $\beta$  (Figure 2A), four transition pairs for pro-IAPP $\gamma$  (Figure 2B), and three transition pairs for fs-IAPP $\gamma$  (Figure 2C). All proteotypic peptides for the hIAPP isoform SRM assay, calibration graphs with linear fitting, correlation coefficient  $R^2$ , and LOQ are shown in the right panel of Figure 2.

We found that pro-IAPP $\gamma$  and fs-IAPP $\gamma$  were at similar levels but only approximately 20% of the level of pro-IAPP $\beta$  in plasma (Figure S2B). We performed a Pearson correlation analysis between IAPP by IAPP-ELISA, which detects IAPP<sub>37</sub> only, and SRM results and found significant correlations of IAPP-ELISA with pro-IAPP $\beta$  ( $r = 0.43, p = 0.02$ ) but not with pro-IAPP $\gamma$  ( $r = 0.03, p = 0.87$ ) or fs-IAPP $\gamma$  ( $r = 0.01, p = 0.95$ ) in the plasma samples ( $n = 28$ ) (Figure S3A). We concluded that hIAPP $\gamma$  is not recognized in plasma by ELISA for IAPP, perhaps because the antibody is specific for mature IAPP<sub>37</sub>.

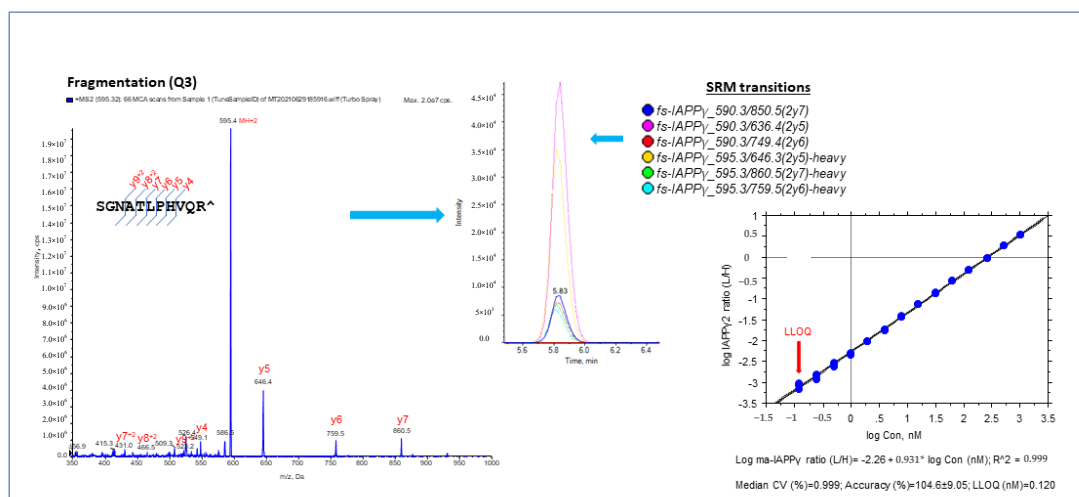


(A)

Figure 2. Cont.



(B)



(C)

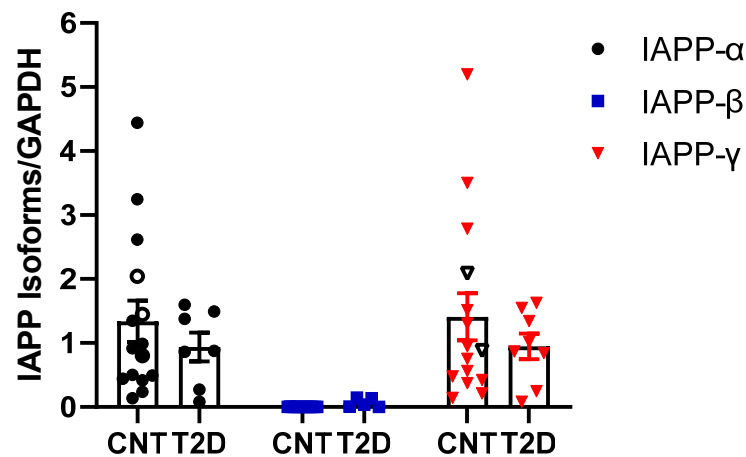
**Figure 2.** Proteotypic peptides for SRM assay of IAPPs. MS/MS spectra generated by SRM reaction of transitions with light or heavy SIS of target peptides, pro-IAPP $\beta$  (A), pro-IAPP $\gamma$  (B), and fs-IAPP $\gamma$  (C) in the (left panels). A set of coeluting peaks in the plasma matrix confirms that the detected SRM signals are derived from each proteotypic peptide in the (middle panels). The quantitative validation of the SRM assay is displayed in the (right panels). The calibration curve of the SRM assay for each proteotypic peptide in the plasma matrix was carried out as follows: (1) linearity was determined by linear regression between the measured peak area ratio of light and heavy SIS versus the theoretical concentration of light-SIS peptide in the plasma matrix prepared from pooled samples; we display the linear regression with the dashed line representing CI (95%) for the mean,  $n = 3$ ; (2) accuracy was estimated by back fitting data to the STD curve from all quantified points ( $>5$  points) in the plots, as expressed as the mean  $\pm$  SD (%); and (3) LLOQ was determined from the standard curve, defined as the lowest concentration with acceptable CV  $< 20\%$  and accuracy within  $100 \pm 20\%$ .

### 3.1.3. hIAPP $\beta$ and hIAPP $\gamma$ in T2DM Islets and AD Cerebrum

We designed TaqMan probes at splicing junctions that specifically hybridize to hIAPP $\alpha$ , hIAPP $\beta$ , and hIAPP $\gamma$  (Figure 1A and Table S1) isoforms and compared their expression in nondiabetic and T2DM islets and non-AD and AD middle temporal gyrus (MTG) that has A $\beta$  burden early in the disease [46] using a sensitive ddPCR method. As expected, hIAPP $\alpha$  was highly expressed in islets, and we also found that hIAPP $\gamma$  expression was at a similar level, while hIAPP $\beta$  mRNA was approximately 0.1% of hIAPP $\alpha$  (Figure 3A). We were able to detect mRNAs of hIAPP $\alpha$  (5 out of 15), hIAPP $\beta$  (14 out of 16), and

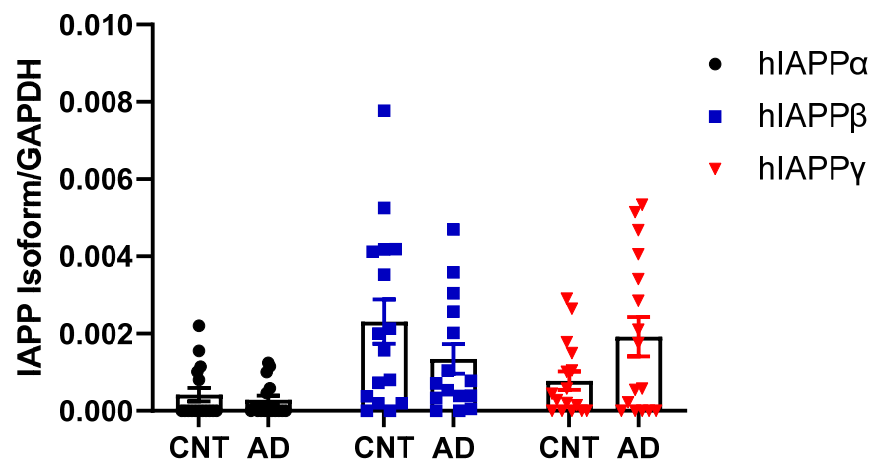
hIAPP $\gamma$  (11 out of 16) at low levels in MTG samples (Figure 3B) using ddPCR. Islet hIAPP $\alpha$  and hIAPP $\gamma$  expression levels were 2990- and 1800-fold higher than those of MTG, respectively. However, hIAPP $\beta$  mRNA level in islets was 44% that of MTG and it was 6-fold higher than that of hIAPP $\alpha$  in human MTG. There were no significant changes at the mRNA level in T2DM islets or AD MTG samples compared to those of controls (Figure 3A,B). At the protein level, pro-IAPP $\gamma$  levels were reduced in T2DM islets to  $15.9 \pm 0.4\%$  ( $t_{(10)} = 2.85$ ,  $p = 0.017$ ) of nondiabetic islets, while there were no differences in pro-IAPP $\beta$  levels (Figure 3C). In contrast, the pro-IAPP $\beta$  quantity was increased 1.27-fold ( $t_{(30)} = 3.11$ ,  $p = 0.004$ ) in the AD MTG compared to the non-AD samples (Figure 3D). We designed a peptide C(Cam)NTATC(Cam)ATQR that is located within IAPP $_{37}$  for our SRM assay; unfortunately, its elution time was less than 2 min, and the transition peaks were not amenable to analyses. The change of IAPP isoform at protein levels in pathological islets and MTG prompted us to investigate whether they could serve as blood-based biomarkers in early AD patients.

### ddPCR of IAPP isoforms in islets



(A)

### ddPCR of hIAPP isoforms in MTG



(B)

Figure 3. Cont.

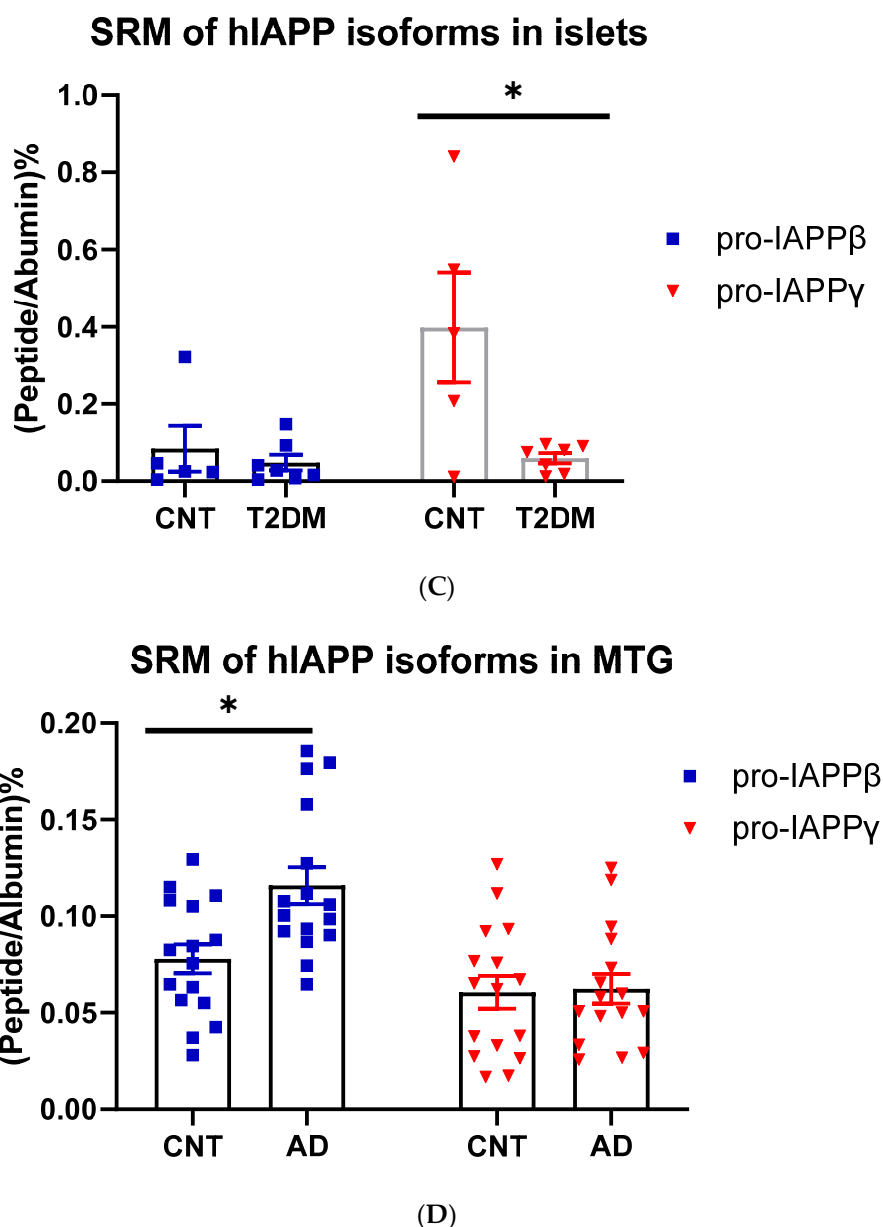


**Figure 3.** IAPP isoform expression in islets and cerebrum. (A) ddPCR of IAPP isoform expression in islets of controls (CNT,  $n = 14$ – $15$ , 12–13 fresh islets of close marks and two frozen of open marks) and type 2 diabetes (T2DM,  $n = 7$ – $8$ ) and (B) in the MTG of controls (CNT,  $n = 15$ – $16$ ) and Alzheimer’s disease (AD,  $n = 15$ – $16$ ). The Y-axis shows droplets of islet IAPP isoforms normalized to those of GAPDH. (C) SRM measurements of pro-IAPP $\beta$  and pro-IAPP $\gamma$  at the peptide level in islets of controls (CNT,  $n = 5$ ) and type 2 diabetes (T2DM,  $n = 7$ ) and (D) in the MTG of controls (CNT,  $n = 16$ ) and Alzheimer’s disease (AD,  $n = 16$ ). The Y-axis is the percentage of IAPP isoform peptides normalized to albumin. \* represents statistically significant ( $p < 0.05$ ).

#### 3.1.4. Reduction of hIAPP $\beta$ and hIAPP $\gamma$ Peptides in AD Plasma Samples

We used partial least squares-discriminant analysis (PLS-DA) to reduce the number of variables in multidimensional SRM data and observed that the proportion of variance was centered in the first two components, i.e., component 1 (C1) explained 56.3% and component 2 (C2) explained 26.4% of the total variance (Figure S3B). Notably, pro-IAPP $\beta$  had the highest loading in C1 and C2. The first two components clearly separated the AD plasma samples from those of controls (Figure S3C). We found that the level of pro-IAPP $\beta$  was nine-fold and two-fold higher than that of pro-IAPP $\gamma$  and fs-IAPP $\gamma$ , respectively. The pro-IAPP $\beta$ , pro-IAPP $\gamma$ , and fs-IAPP $\gamma$  in AD plasma samples were reduced to 56.5%

( $t_{(27)} = 4.65, p < 0.0001$ ), 82.0% ( $t_{(27)} = 2.41, p = 0.0229$ ), and 72.6% ( $t_{(27)} = 2.42, p = 0.0224$ ) of those in normal controls, respectively (Figure 4A–C), but we did not find significant differences ( $t_{(26)} = 0.25, p = 0.8044$ ) by IAPP-ELISA (Figure 4D). We further evaluated the detection accuracy of hIAPP isoforms as plasma-based AD biomarkers using ROC analysis. We found that pro-IAPP $\beta$ , pro-IAPP $\gamma$ , and fs-IAPP $\gamma$  determined by SRM could effectively discriminate between AD and controls, with AUROC values of 0.89 ( $p = 0.0006$ ), 0.77 ( $p = 0.018$ ), and 0.75 ( $p = 0.028$ ), respectively (Figure 4E–G), while the performance of the IAPP-ELISA was like chance, with an AUROC of 0.51 ( $p = 0.93$ ) (Figure 4H). In CSF, the hIAPP isoforms were detectable but below the lower limit of quantification (LLOQ) using SRM.

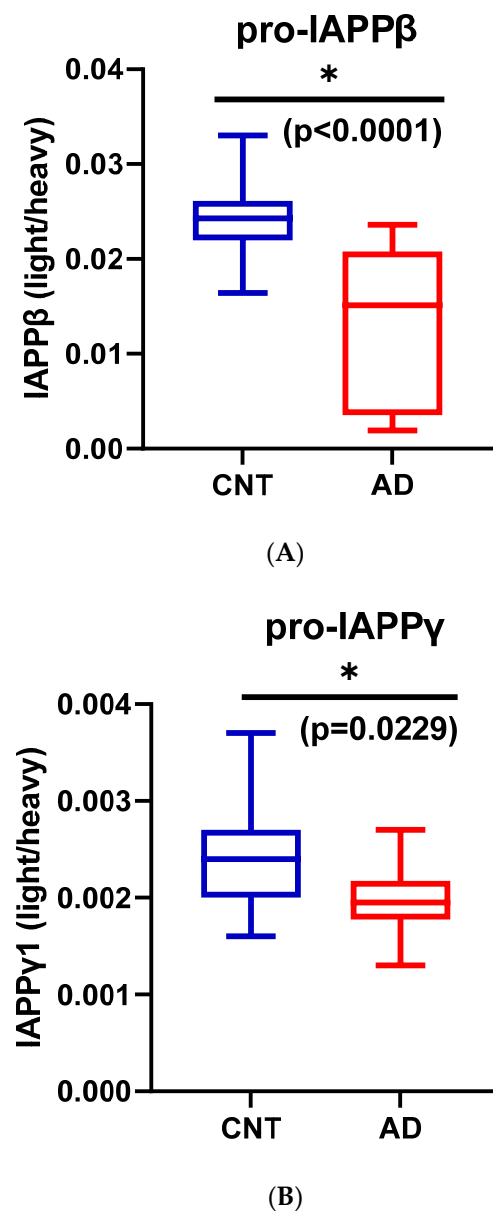
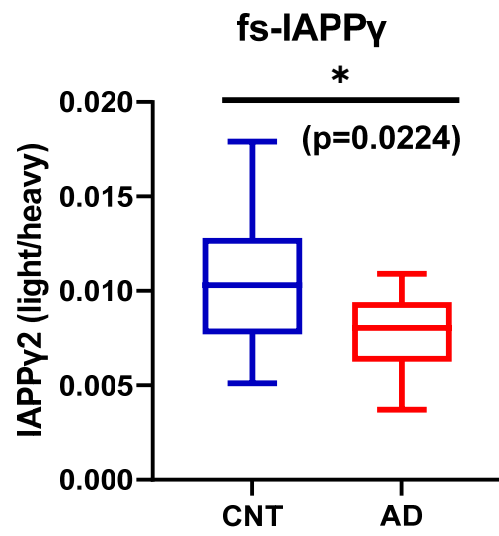
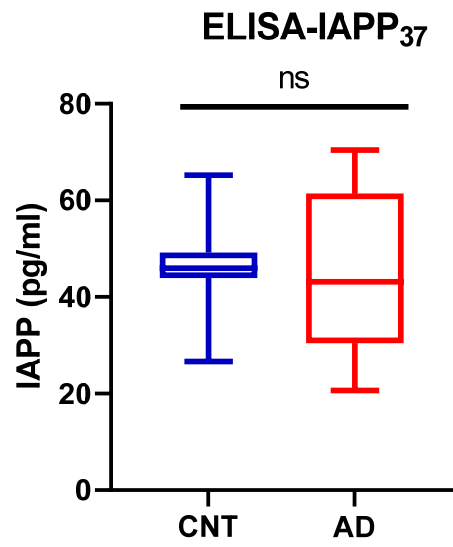


Figure 4. Cont.

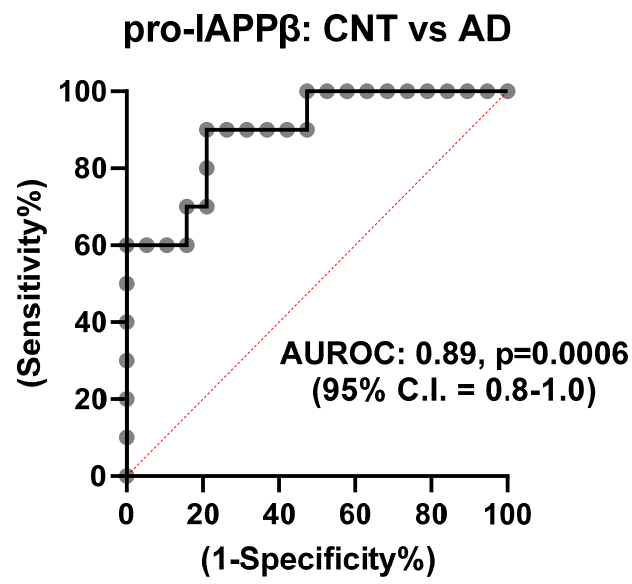


(C)

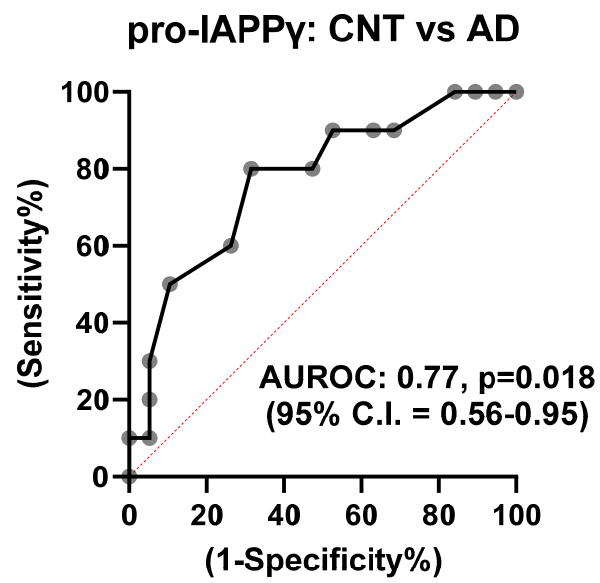


(D)

Figure 4. Cont.



(E)



(F)

Figure 4. Cont.

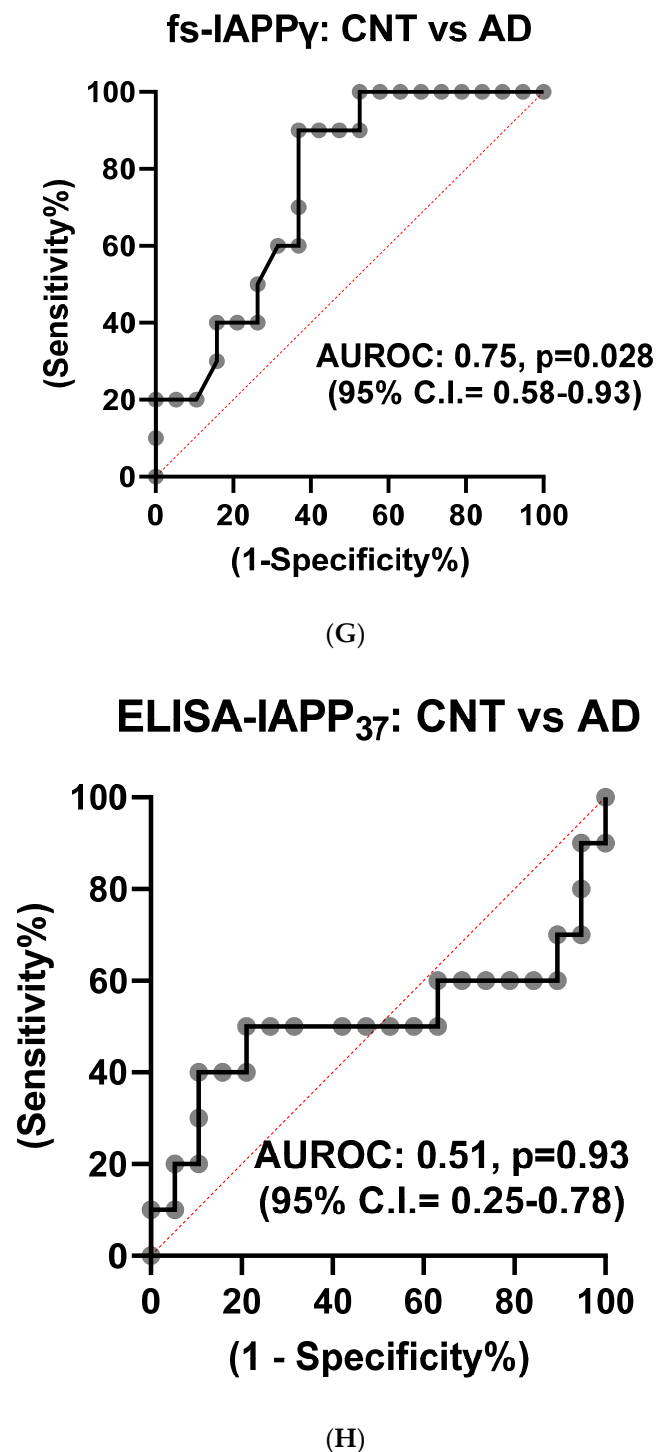
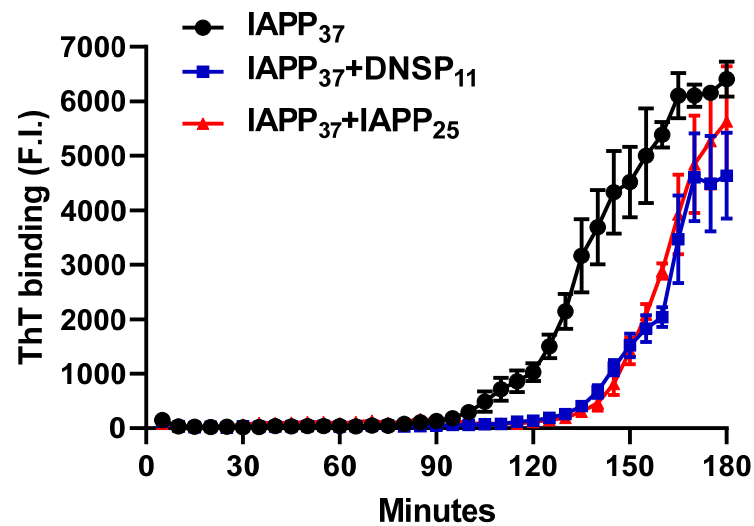


**Figure 4.** IAPP isoform peptide concentrations in control and AD plasma samples. Unpaired Student's *t*-tests: (A) pro-IAPP $\beta$ ; (B) pro-IAPP $\gamma$ ; (C) fs-IAPP $\gamma$ ; (D) IAPP-ELISA. The Y-axis is the ratio of peak area (light/heavy) for SRM and pg/mL for ELISA. Area under the receiver operating characteristic curve (AUROC) tests: (E) pro-IAPP $\beta$ ; (F) pro-IAPP $\gamma$ ; (G) fs-IAPP $\gamma$ ; (H) IAPP-ELISA. The Y-axis is the true positive rate, and the X-axis is the true negative rate. ns: not significant.

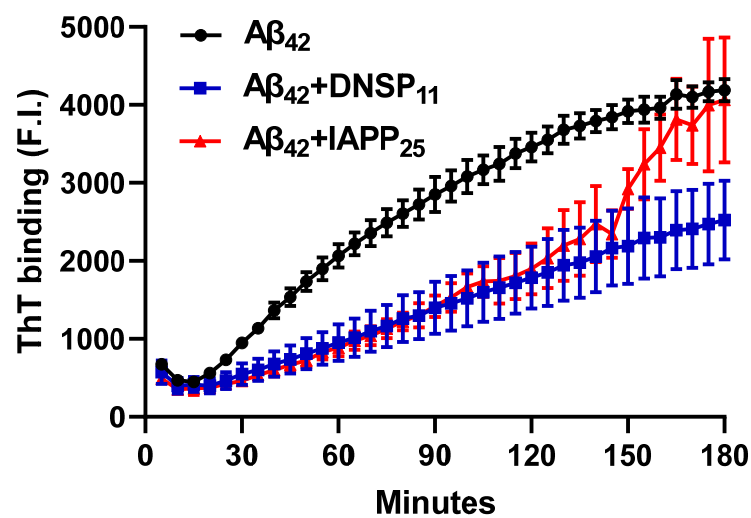
### 3.1.5. In Vitro Inhibition of IAPP $_{37}$ and Ab $_{42}$ Fibrillation by IAPP $_{25}$ and DNSP $_{11}$

We tested whether DNSP $_{11}$  and newly discovered IAPP $_{25}$  peptide impacted A $\beta_{42}$  and IAPP $_{37}$  aggregation using Thioflavin T assay. Figure 5A is a representative experiment showing IAPP $_{37}$  aggregation dynamics with a lag time of 90 min and inhibition by equal molar amounts of IAPP $_{25}$  (derived from hIAPP $\gamma$ ) and DNSP $_{11}$ . We found that IAPP $_{37}$  ag-

gregation was inhibited by both IAPP<sub>25</sub> and DNSP<sub>11</sub> (25.0% and 24.1% of IAPP aggregation dynamics, respectively;  $p = 0.003$ ) in the linear range of 90–160 min (Figure 5F). This finding implies that the reduction of IAPP<sub>25</sub> in T2DM islets observed in Figure 3C might disinhibit IAPP fibrillation in T2DM islets, and DNSP<sub>11</sub> might play a protective role in islets as it was shown in substantial nigra of brain [47].

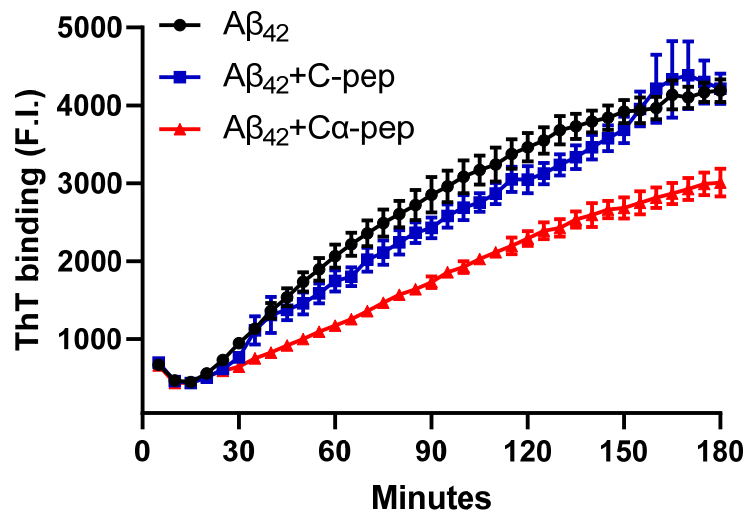


(A)

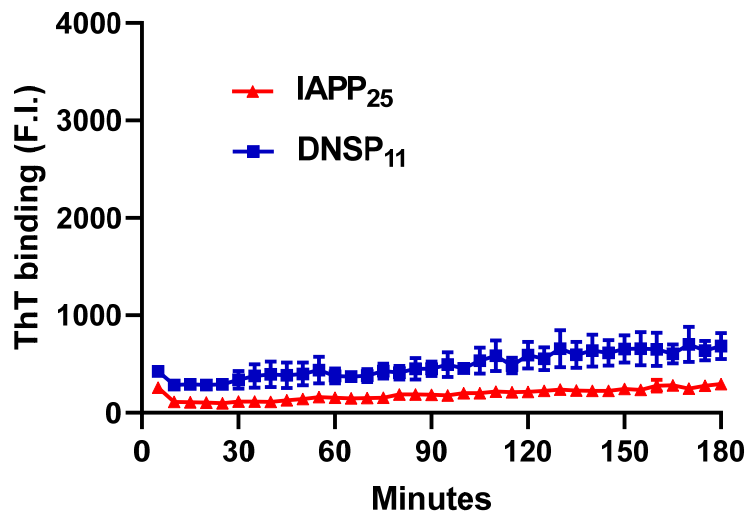


(B)

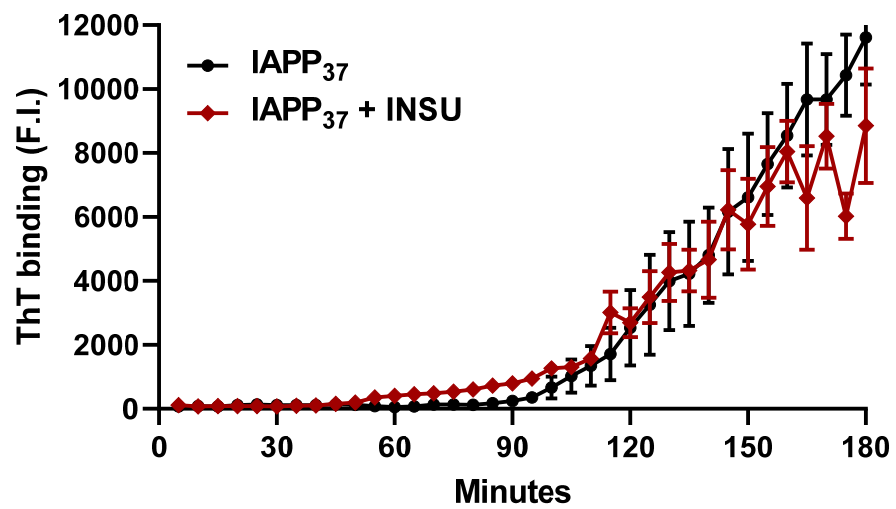
Figure 5. Cont.



(C)

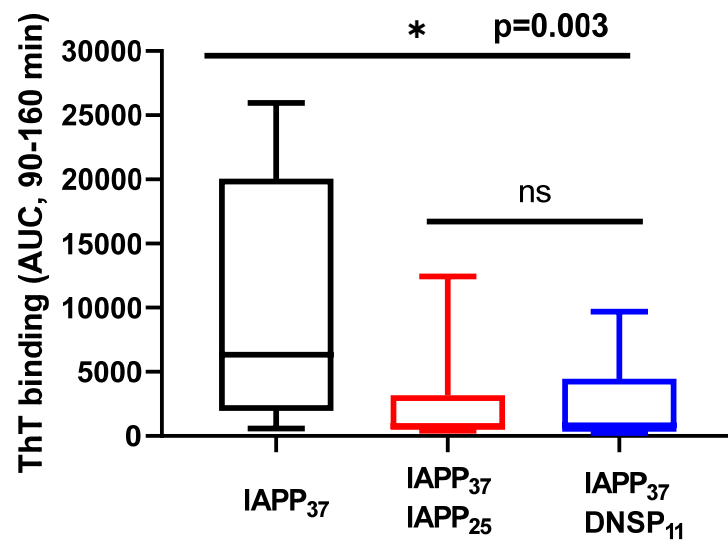


(D)

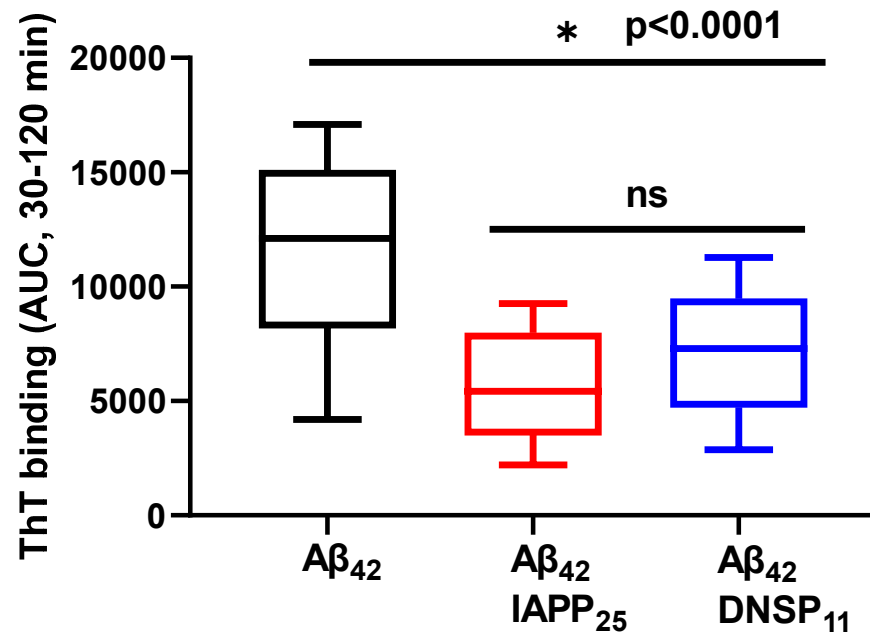


(E)

Figure 5. Cont.



(F)



(G)

Figure 5. Cont.

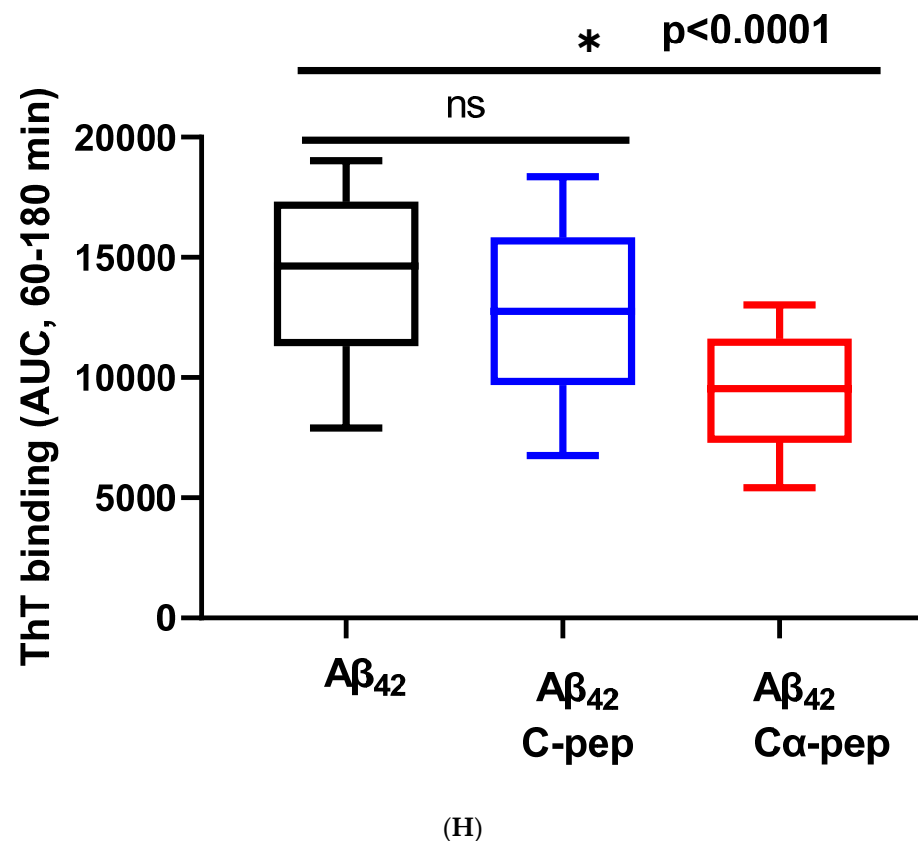


**Figure 5.** Inhibition of IAPP<sub>37</sub> and Aβ<sub>42</sub> fibrillation by IAPP<sub>25</sub>, DNSP<sub>11</sub>, and Cα-peptide. Y-axis represents the fluorescence intensity (F.I) of ThT binding and X-axis minutes. Representative fibrillation dynamics and inhibition curves in three replicates for (A) IAPP<sub>37</sub> with equal molar concentration of IAPP<sub>25</sub> and DNSP<sub>11</sub>; (B) Aβ<sub>42</sub> with equal molar concentration of IAPP<sub>25</sub> and DNSP<sub>11</sub>; (C) with equal molar concentration of C- and Cα-peptides; (D) thioflavin T (ThT) amyloid reporter assay of IAPP<sub>25</sub> and DNSP<sub>11</sub>; IAPP<sub>25</sub> or DNSP<sub>11</sub> alone did not bind to the ThT amyloid reporter. (E) No inhibition of IAPP<sub>37</sub> fibrillation by insulin upstream open reading frame peptide occurs (INSU). Box-whisker plot of the inhibition. Y-axis is the area under the curve (AUC) of ThT fluorescence intensity. (F) Inhibition of IAPP<sub>37</sub> fibrillation by IAPP<sub>25</sub> and DNSP<sub>11</sub> in the range of 90–160 min. (G) Inhibition of Aβ<sub>42</sub> fibrillation by IAPP<sub>25</sub> and by DNSP<sub>11</sub> in the range of 30–120 min and (H) by C- and Cα-peptide in the range of 60–180 min. ns: not significant.

The Aβ<sub>42</sub> aggregation with a lag time of 20 min was also inhibited by equal molar amounts of IAPP<sub>25</sub> and DNSP<sub>11</sub> (Figure 5B) with 49.0 and 61.9% of Aβ aggregation dynamics, respectively, ( $p < 0.0001$ ) in the linear range of 30–120 min (Figure 5G). The Aβ<sub>42</sub> aggregation was inhibited by Cα-peptide (66.5% of Aβ<sub>42</sub> aggregation dynamics) shown previously to inhibit IAPP<sub>37</sub> fibril formation in vitro [9] but not inhibited by C-peptide (Figure 5C,H). IAPP<sub>37</sub> aggregation was not affected by the equal molar amounts of the uORF of INSU peptide [9] used as a negative control (Figure 5D). All these suggest that equal molar ratio used in our experiments likely does not jeopardize the specificity of the observed inhibitory effects of DNSP<sub>11</sub> and IAPP<sub>25</sub>.

#### 4. Discussion

We uncovered two novel hominid-specific hIAPP isoforms derived from four exons instead of the conventional three exons. The hIAPPβ isoform has a 14-AA insertion in the N-terminal prohormone region of hIAPPα, but it is processed to the same mature IAPP<sub>37</sub>. The hIAPPγ isoform, on the other hand, has a different prohormone sequence from hIAPPα and a frameshifted preproIAPP that is processed to a nonaggregating peptide (IAPP<sub>25</sub>). IAPP belongs to a group of rapidly evolving genes known to have new primate-specific

exons [48,49]. For example, coding sequences of exon 4 of hIAPP $\gamma$  are conserved only in humans, Neanderthals, chimps, and gorillas, and exon 5 of hIAPP $\beta$  is conserved in hominids, including gibbons. The *IAPP* gene is one of the most human tissue-specific expressed genes, reportedly predominantly present in  $\beta$ -cells, although we found low levels of IAPP isoforms in human testes, including a hominid-specific upstream exon 1. hIAPP $\beta$  expression was higher in human cerebrum than in islets, resembling the chicken IAPP gene that is predominantly expressed in the brain [50], indicating that new exons might contribute to yet unknown neuroendocrine functions. On the other hand, hIAPP $\alpha$  and hIAPP $\gamma$  expressions in islets are more than a thousand-fold higher than those in the MTG. That the hIAPP $\beta$  peptide level was higher in plasma than that of hIAPP $\gamma$  implied the presence of hIAPP $\beta$  in gastrointestinal glands [51]. Direct comparison of SRM values of hIAPP $\alpha$  with hIAPP $\gamma$  was hampered by the short elution time (<2 min) of the amyloidogenic peptide for IAPP<sub>37</sub> (CNTATCATQR) and the different absolute values of IAPP<sub>25</sub> SRM and ELISA-IAPP<sub>37</sub> in plasma [52]. SRM is supported by physical reactions that do not depend on antibody and epitope specificity. The LOQ differences of SRM and ELISA are more than 10-fold [53], so it is not possible to compare ELISA IAPP<sub>37</sub> to SRM IAPP<sub>25</sub> ratio in islets and plasma. We are currently developing IAPP<sub>25</sub> antibody to compare IAPP<sub>25</sub> and IAPP<sub>37</sub> ratio with ELISA and Western Blot. Due to primate evolution favoring phenotypic longevity and intelligence, human-specific genome adaptation, either beneficial or adverse, is intimately associated with metabolic and tissue degenerative diseases. For instance, the human-specific APOE e3 allele arose approximately 220,000 and e2 approximately 80,000 years ago, perhaps mitigating any inherent cognitive adverse effects of the ancestral e4 allele [54] (also the major genetic risk factor for sporadic AD) [55,56]. In the same vein, new intra-exonal splicing of the human *INS* gene created the C $\alpha$ -peptide that slows the rate of IAPP and A $\beta$  fibrillation [9]; mutations of a primate specific gene ZNF808 cause neonatal diabetes due to pancreatic agenesis [57]; overexpression of human antisense transcripts of BDNF (BDNFOS) increases  $\beta$ -site APP cleaving enzyme 1 (BACE1) activity that can result in AD [15,58]; overexpression of human antisense transcripts of GDNF (GDNFOS1) occurs in AD brain [15] and unfortunately enhances the viability of glioblastoma cells [15,59], and upregulation of the human de novo gene FLJ33706 also occurs in the AD brain [60]. We now find that the hominid-specific hIAPP $\gamma$  inhibits IAPP<sub>37</sub> fibrillation; therefore, reduced hIAPP $\gamma$  could accelerate IAPP aggregation in islets. On the other hand, increased hIAPP $\beta$  levels in the MTG leading to amyloidogenic IAPP<sub>37</sub> could seed amyloidosis in the AD brain.

GDNF is highly expressed in  $\alpha$ -cells of islets and is downregulated in AD brain regions [15,18]. GDNF sustains dopaminergic (DA) neurons and prevents their death in Parkinson's disease (PD) [13]. DNSP<sub>11</sub> derived from proGDNF $\alpha$  is localized in the substantia nigra and inhibits 6-hydroxydopamine-induced toxicity of dopamine neurons [19]. In addition, serum GDNF levels are significantly lower in T2DM [61]. However, there is no study on the role of DNSP<sub>11</sub> in amyloid formation, whether  $\alpha$ -synuclein is involved in Lewy body disease, A $\beta$  is involved in AD, or IAPP is involved in islets in T2DM. Various peptides derived from IAPP, insulin, C-peptide, and chromogranin A have been developed to inhibit IAPP fibrillation [62].

Finally, it remains a challenge to develop cost-effective and noninvasive blood-based biomarkers to diagnose preclinical AD before extensive neuronal death occurs [63]. Previous studies by Adler et al. [25] and Zhu et al. [26] reported that IAPP<sub>37</sub> is significantly reduced in AD plasma samples by ELISA, and our IAPP-ELISA did not reproduce their findings. The discrepancy of the SRM from the previous ELISA may be because our participants were a cohort with early AD symptoms. In this study, we used our SRM assay, achieving high diagnostic accuracy. This is especially the case for pro-IAPP $\beta$ , with an AUROC of 0.89, which is in the range of accuracy for the most advanced immune assays for markers considered central to AD pathogenesis, such as A $\beta$  (0.78) [64], soluble A $\beta$  oligomers (0.89) [65], pTau<sub>217</sub> (0.98), pTau<sub>181</sub> (0.97) [66], N-terminal Tau fragment (0.95) [67], total Tau (0.78), and neurofilament light (0.87) [68] or even neuronal-derived extracellular vesicles (0.89) [69], which have been proposed as predictors of future AD

diagnosis [70]. Given the limited number of plasma samples (19 controls and 10 individuals with AD) examined, the diagnostic performance of the hIAPP $\beta$  and hIAPP $\gamma$  SRM assays should be further validated in larger studies for clinical relevance since IAPP<sub>37</sub> is known to enter the brain and may be involved in seeding of A $\beta$  amyloid.

## 5. Conclusions

We uncovered hominid-specific peptides derived from IAPP isoforms that potentially could be developed as blood-based biomarkers for early AD and have use as peptide-based anti-amyloid drugs.

**Supplementary Materials:** The following supporting information can be downloaded at: <https://www.mdpi.com/article/10.3390/biom13010167/s1>, Table S1 (TaqMan probe and primer sequences of human IAPP isoforms) and S2 (Unlabeled and stable isotope labeled IAPP $\beta$  and IAPP $\gamma$  isoform tryptic peptide sequences); Figure S1 (IAPP exon ortholog nucleotide sequence alignments), Figure S2 (hIAPP isoform mRNA levels in islets and testis; and pro-IAPP $\beta$  and pro-IAPP $\gamma$  peptide levels in plasma samples, and Figure S3 (Statistical analysis of hIAPP isoform peptide levels in human plasma samples).

**Author Contributions:** Q.-R.L. and J.M.E. conceptualized the study and wrote the manuscript. Q.-R.L. performed the bioinformatics search and molecular biological experiments. M.Z. designed and performed SRM experiments, and Q.C. performed ELISA. M.M. and D.K. collected plasma and CSF samples from AD patients and controls. M.Z. and Q.-R.L. analyzed the qPCR and SRM data. All authors have read and agreed to the published version of the manuscript.

**Funding:** This work was funded by the Intramural Research Program (IRP) of the National Institute on Aging (JME: 1T ZIAAct AG000455, Deconstructing insulin in the brain in relation to Alzheimer's Disease).

**Institutional Review Board Statement:** Plasma and cerebrospinal fluid (CSF) samples were from the IRB-approved study of NCT01255163 and the protocols 10AG0423, approved through 27 October 2022; and 03-AG-0325, approved through 5 October 2022.

**Informed Consent Statement:** Informed consent was obtained from all subjects involved in the study.

**Data Availability Statement:** The IAPP isoform cDNA clones for hIAPP-a and hIAPP-g, tryptic peptides, and TaqMan probes are available upon request.

**Acknowledgments:** We thank Olga Pletnikova and Juan C. Troncoso of Departments of Pathology, Neuropathology Division, Johns Hopkins University School of Medicine for providing postmortem middle temporal gyrus (MTG) of pathologically confirmed AD and non-AD samples for this study.

**Conflicts of Interest:** The authors declare no conflict of interest.

## References

1. Raleigh, D.; Zhang, X.; Hastoy, B.; Clark, A. The beta-cell assassin: IAPP cytotoxicity. *J. Mol. Endocrinol.* **2017**, *59*, R121–R140. [[CrossRef](#)] [[PubMed](#)]
2. Westermark, P. Amyloid in the islets of Langerhans: Thoughts and some historical aspects. *Ups. J. Med. Sci.* **2011**, *116*, 81–89. [[CrossRef](#)]
3. Fortin, J.S.; Benoit-Biancamano, M.O. Wildlife sequences of islet amyloid polypeptide (IAPP) identify critical species variants for fibrillization. *Amyloid* **2015**, *22*, 194–202. [[CrossRef](#)]
4. Bhowmick, D.C.; Singh, S.; Trikha, S.; Jeremic, A.M. The Molecular Physiopathogenesis of Islet Amyloidosis. *Handb. Exp. Pharmacol.* **2018**, *245*, 271–312. [[PubMed](#)]
5. Milardi, D.; Gazit, E.; Radford, S.E.; Xu, Y.; Gallardo, R.U.; Cafilisch, A.; Westermark, G.T.; Westermark, P.; Rosa, C.; Ramamoorthy, A. Proteostasis of Islet Amyloid Polypeptide: A Molecular Perspective of Risk Factors and Protective Strategies for Type II Diabetes. *Chem. Rev.* **2021**, *121*, 1845–1893. [[CrossRef](#)] [[PubMed](#)]
6. Liu, Q.R.; Aseer, K.R.; Yao, Q.; Zhong, X.; Ghosh, P.; O'Connell, J.F.; Egan, J.M. Anti-Inflammatory and Pro-Autophagy Effects of the Cannabinoid Receptor CB2R: Possibility of Modulation in Type 1 Diabetes. *Front. Pharmacol.* **2021**, *12*, 809965. [[CrossRef](#)] [[PubMed](#)]
7. Segerstolpe, A.; Palasantza, A.; Eliasson, P.; Andersson, E.M.; Andreasson, A.C.; Sun, X.; Picelli, S.; Sabirsh, A.; Clausen, M.; Bjursell, M.K.; et al. Single-Cell Transcriptome Profiling of Human Pancreatic Islets in Health and Type 2 Diabetes. *Cell Metab.* **2016**, *24*, 593–607. [[CrossRef](#)]

8. Kudva, Y.C.; Mueske, C.; Butler, P.C.; Eberhardt, N.L. A novel assay in vitro of human islet amyloid polypeptide amyloidogenesis and effects of insulin secretory vesicle peptides on amyloid formation. *Biochem. J.* **1998**, *331 Pt 3*, 809–813. [[CrossRef](#)]
9. Liu, Q.R.; Zhu, M.; Zhang, P.; Mazucanti, C.H.; Huang, N.S.; Lang, D.L.; Chen, Q.; Auluck, P.; Marenco, S.; O’Connell, J.F.; et al. Novel Human Insulin Isoforms and Calpha-Peptide Product in Islets of Langerhans and Choroid Plexus. *Diabetes* **2021**, *70*, 2947–2956. [[CrossRef](#)]
10. Chen, Y.C.; Taylor, A.J.; Verchere, C.B. Islet prohormone processing in health and disease. *Diabetes Obes. Metab.* **2018**, *20* (Suppl. S2), 64–76. [[CrossRef](#)]
11. Clark, A.; Nilsson, M.R. Islet amyloid: A complication of islet dysfunction or an aetiological factor in Type 2 diabetes? *Diabetologia* **2004**, *47*, 157–169. [[CrossRef](#)] [[PubMed](#)]
12. Asthana, S.; Mallick, B.; Alexandrescu, A.T.; Jha, S. IAPP in type II diabetes: Basic research on structure, molecular interactions, and disease mechanisms suggests potential intervention strategies. *Biochim. Biophys. Acta Biomembr.* **2018**, *1860*, 1765–1782. [[CrossRef](#)] [[PubMed](#)]
13. Barker, R.A.; Bjorklund, A.; Gash, D.M.; Whone, A.; Van Laar, A.; Kordower, J.H.; Bankiewicz, K.; Kieburtz, K.; Saarma, M.; Booms, S.; et al. GDNF and Parkinson’s Disease: Where Next? A Summary from a Recent Workshop. *J. Parkinsons. Dis.* **2020**, *10*, 875–891. [[CrossRef](#)] [[PubMed](#)]
14. Ito, Y.; Okada, Y.; Sato, M.; Sawai, H.; Funahashi, H.; Murase, T.; Hayakawa, T.; Manabe, T. Expression of glial cell line-derived neurotrophic factor family members and their receptors in pancreatic cancers. *Surgery* **2005**, *138*, 788–794. [[CrossRef](#)]
15. Airavaara, M.; Pletnikova, O.; Doyle, M.E.; Zhang, Y.E.; Troncoso, J.C.; Liu, Q.R. Identification of novel GDNF isoforms and cis-antisense GDNFOS gene and their regulation in human middle temporal gyrus of Alzheimer disease. *J. Biol. Chem.* **2011**, *286*, 45093–45102. [[CrossRef](#)]
16. Mwangi, S.; Anitha, M.; Mallikarjun, C.; Ding, X.; Hara, M.; Parsadarian, A.; Larsen, C.P.; Thule, P.; Sitaraman, S.V.; Anania, F.; et al. Glial cell line-derived neurotrophic factor increases beta-cell mass and improves glucose tolerance. *Gastroenterology* **2008**, *134*, 727–737. [[CrossRef](#)]
17. Mwangi, S.M.; Usta, Y.; Raja, S.M.; Anitha, M.; Chandrasekharan, B.; Parsadarian, A.; Sitaraman, S.V.; Srinivasan, S. Glial cell line-derived neurotrophic factor enhances neurogenin3 gene expression and beta-cell proliferation in the developing mouse pancreas. *Am. J. Physiol. Gastrointest Liver Physiol.* **2010**, *299*, G283–G292. [[CrossRef](#)]
18. Lucini, C.; Maruccio, L.; Facello, B.; Cocchia, N.; Tortora, G.; Castaldo, L. Cellular localization of GDNF and its GFRalpha1/RET receptor complex in the developing pancreas of cat. *J. Anat.* **2008**, *213*, 565–572. [[CrossRef](#)]
19. Bradley, L.H.; Fuqua, J.; Richardson, A.; Turchan-Cholewo, J.; Ai, Y.; Kelps, K.A.; Glass, J.D.; He, X.; Zhang, Z.; Grondin, R.; et al. Dopamine neuron stimulating actions of a GDNF propeptide. *PLoS ONE* **2010**, *5*, e9752. [[CrossRef](#)]
20. Immonen, T.; Alakuijala, A.; Hytonen, M.; Sainio, K.; Poteryaev, D.; Saarma, M.; Pasternack, M.; Sariola, H. A proGDNF-related peptide BEP increases synaptic excitation in rat hippocampus. *Exp. Neurol.* **2008**, *210*, 793–796. [[CrossRef](#)]
21. Stenslik, M.J.; Potts, L.F.; Sonne, J.W.; Cass, W.A.; Turchan-Cholewo, J.; Pomerleau, F.; Huettl, P.; Ai, Y.; Gash, D.M.; Gerhardt, G.A.; et al. Methodology and effects of repeated intranasal delivery of DNSP-11 in a rat model of Parkinson’s disease. *J. Neurosci. Methods* **2015**, *251*, 120–129. [[CrossRef](#)] [[PubMed](#)]
22. Jackson, K.; Barisone, G.A.; Diaz, E.; Jin, L.W.; DeCarli, C.; Despa, F. Amylin deposition in the brain: A second amyloid in Alzheimer disease? *Ann. Neurol.* **2013**, *74*, 517–526. [[CrossRef](#)] [[PubMed](#)]
23. Hu, R.; Zhang, M.; Chen, H.; Jiang, B.; Zheng, J. Cross-Seeding Interaction between beta-Amyloid and Human Islet Amyloid Polypeptide. *ACS Chem. Neurosci.* **2015**, *6*, 1759–1768. [[CrossRef](#)]
24. Moreno-Gonzalez, I.; Edwards Iii, G.; Salvadores, N.; Shahnawaz, M.; Diaz-Espinoza, R.; Soto, C. Molecular interaction between type 2 diabetes and Alzheimer’s disease through cross-seeding of protein misfolding. *Mol. Psychiatry* **2017**, *22*, 1327–1334. [[CrossRef](#)] [[PubMed](#)]
25. Adler, B.L.; Yarchoan, M.; Hwang, H.M.; Louneva, N.; Blair, J.A.; Palm, R.; Smith, M.A.; Lee, H.G.; Arnold, S.E.; Casadesus, G. Neuroprotective effects of the amylin analogue pramlintide on Alzheimer’s disease pathogenesis and cognition. *Neurobiol. Aging* **2014**, *35*, 793–801. [[CrossRef](#)]
26. Zhu, H.; Tao, Q.; Ang, T.F.A.; Massaro, J.; Gan, Q.; Salim, S.; Zhu, R.Y.; Kolachalama, V.B.; Zhang, X.; Devine, S.; et al. Association of Plasma Amylin Concentration With Alzheimer Disease and Brain Structure in Older Adults. *JAMA Netw. Open* **2019**, *2*, e199826. [[CrossRef](#)]
27. Makimattila, S.; Fineman, M.S.; Yki-Jarvinen, H. Deficiency of total and nonglycosylated amylin in plasma characterizes subjects with impaired glucose tolerance and type 2 diabetes. *J. Clin. Endocrinol. Metab.* **2000**, *85*, 2822–2827. [[CrossRef](#)]
28. Zhu, H.; Stern, R.A.; Tao, Q.; Bourlas, A.; Esis, M.D.; Chivukula, M.; Rosenzweig, J.; Steenkamp, D.; Xia, W.; Mercier, G.A.; et al. An amylin analog used as a challenge test for Alzheimer’s disease. *Alzheimers Dement.* **2017**, *3*, 33–43. [[CrossRef](#)]
29. Zhu, H.; Xue, X.; Wang, E.; Wallack, M.; Na, H.; Hooker, J.M.; Kowall, N.; Tao, Q.; Stein, T.D.; Wolozin, B.; et al. Amylin receptor ligands reduce the pathological cascade of Alzheimer’s disease. *Neuropharmacology* **2017**, *119*, 170–181. [[CrossRef](#)]
30. Garcia-Vinuales, S.; Ilie, I.M.; Santoro, A.M.; Romanucci, V.; Zarrelli, A.; Di Fabio, G.; Caflich, A.; Milardi, D. Silybins inhibit human IAPP amyloid growth and toxicity through stereospecific interactions. *Biochim. Biophys. Acta Proteins Proteom.* **2022**, *1870*, 140772. [[CrossRef](#)]

31. Sciacca, M.F.M.; Romanucci, V.; Zarrelli, A.; Monaco, I.; Lolicato, F.; Spinella, N.; Galati, C.; Grasso, G.; D'Urso, L.; Romeo, M.; et al. Inhibition of Abeta Amyloid Growth and Toxicity by Silybins: The Crucial Role of Stereochemistry. *ACS Chem. Neurosci.* **2017**, *8*, 1767–1778. [[CrossRef](#)]
32. Leibson, C.L.; Rocca, W.A.; Hanson, V.A.; Cha, R.; Kokmen, E.; O'Brien, P.C.; Palumbo, P.J. Risk of dementia among persons with diabetes mellitus: A population-based cohort study. *Am. J. Epidemiol.* **1997**, *145*, 301–308. [[CrossRef](#)] [[PubMed](#)]
33. Ott, A.; Stolk, R.P.; Hofman, A.; van Harskamp, F.; Grobbee, D.E.; Breteler, M.M. Association of diabetes mellitus and dementia: The Rotterdam Study. *Diabetologia* **1996**, *39*, 1392–1397. [[CrossRef](#)]
34. Mullins, R.J.; Mustapic, M.; Chia, C.W.; Carlson, O.; Gulyani, S.; Tran, J.; Li, Y.; Mattson, M.P.; Resnick, S.; Egan, J.M.; et al. A Pilot Study of Exenatide Actions in Alzheimer's Disease. *Curr. Alzheimer. Res.* **2019**, *16*, 741–752. [[CrossRef](#)] [[PubMed](#)]
35. Sperling, R.A.; Aisen, P.S.; Beckett, L.A.; Bennett, D.A.; Craft, S.; Fagan, A.M.; Iwatsubo, T.; Jack, C.R., Jr.; Kaye, J.; Montine, T.J.; et al. Toward defining the preclinical stages of Alzheimer's disease: Recommendations from the National Institute on Aging-Alzheimer's Association workgroups on diagnostic guidelines for Alzheimer's disease. *Alzheimer's Dement. J. Alzheimer's Assoc.* **2011**, *7*, 280–292. [[CrossRef](#)] [[PubMed](#)]
36. Shaw, L.M.; Vanderstichele, H.; Knapik-Czajka, M.; Clark, C.M.; Aisen, P.S.; Petersen, R.C.; Blennow, K.; Soares, H.; Simon, A.; Lewczuk, P.; et al. Cerebrospinal fluid biomarker signature in Alzheimer's disease neuroimaging initiative subjects. *Annals. Neurol.* **2009**, *65*, 403–413. [[CrossRef](#)]
37. Wilkins, M.R.; Gasteiger, E.; Bairoch, A.; Sanchez, J.C.; Williams, K.L.; Appel, R.D.; Hochstrasser, D.F. Protein identification and analysis tools in the ExPASy server. *Methods Mol. Biol.* **1999**, *112*, 531–552.
38. Mazucanti, C.H.; Liu, Q.R.; Lang, D.; Huang, N.; O'Connell, J.F.; Camandola, S.; Egan, J.M. Insulin is produced in choroid plexus and its release is regulated by serotonergic signaling. *JCI Insight* **2019**, *4*, e131682. [[CrossRef](#)]
39. Liu, Q.R.; Rubio, F.J.; Bossert, J.M.; Marchant, N.J.; Fanous, S.; Hou, X.; Shaham, Y.; Hope, B.T. Detection of molecular alterations in methamphetamine-activated Fos-expressing neurons from a single rat dorsal striatum using fluorescence-activated cell sorting (FACS). *J. Neurochem.* **2014**, *128*, 173–185. [[CrossRef](#)]
40. Majbour, N.; Aasly, J.; Abdi, I.; Ghanem, S.; Erskine, D.; van de Berg, W.; El-Agnaf, O. Disease-Associated alpha-Synuclein Aggregates as Biomarkers of Parkinson Disease Clinical Stage. *Neurology* **2022**, *99*, e2417–e2427.
41. Chia, C.W.; Odetunde, J.O.; Kim, W.; Carlson, O.D.; Ferrucci, L.; Egan, J.M. GIP contributes to islet trihormonal abnormalities in type 2 diabetes. *J. Clin. Endocrinol. Metab.* **2014**, *99*, 2477–2485. [[CrossRef](#)]
42. Boguski, M.S.; Lowe, T.M.; Tolstoshev, C.M. dbEST-database for "expressed sequence tags". *Nat. Genet.* **1993**, *4*, 332–333. [[CrossRef](#)] [[PubMed](#)]
43. Christmanson, L.; Rorsman, F.; Stenman, G.; Westermark, P.; Betsholtz, C. The human islet amyloid polypeptide (IAPP) gene. Organization, chromosomal localization and functional identification of a promoter region. *FEBS Lett.* **1990**, *267*, 160–166. [[CrossRef](#)] [[PubMed](#)]
44. Prufer, K.; Racimo, F.; Patterson, N.; Jay, F.; Sankararaman, S.; Sawyer, S.; Heinze, A.; Renaud, G.; Sudmant, P.H.; de Filippo, C.; et al. The complete genome sequence of a Neanderthal from the Altai Mountains. *Nature* **2014**, *505*, 43–49. [[CrossRef](#)] [[PubMed](#)]
45. Artenstein, A.W.; Opal, S.M. Proprotein convertases in health and disease. *N. Engl. J. Med.* **2011**, *365*, 2507–2518. [[CrossRef](#)] [[PubMed](#)]
46. Villemagne, V.L.; Dore, V.; Bourgeat, P.; Burnham, S.C.; Laws, S.; Salvado, O.; Masters, C.L.; Rowe, C.C. Abeta-amyloid and Tau Imaging in Dementia. *Semin. Nucl. Med.* **2017**, *47*, 75–88. [[CrossRef](#)]
47. Fuqua, J.L.; Littrell, O.M.; Lundblad, M.; Turchan-Cholewo, J.; Abdelmoti, L.G.; Galperin, E.; Bradley, L.H.; Cass, W.A.; Gash, D.M.; Gerhard, G.A. Dynamic changes in dopamine neuron function after DNSP-11 treatment: Effects in vivo and increased ERK 1/2 phosphorylation in vitro. *Peptides* **2014**, *54*, 1–8. [[CrossRef](#)]
48. Liu, Q.R.; Pan, C.H.; Hishimoto, A.; Li, C.Y.; Xi, Z.X.; Llorente-Berzal, A.; Viveros, M.P.; Ishiguro, H.; Arinami, T.; Onaivi, E.S.; et al. Species differences in cannabinoid receptor 2 (CNR2) gene: Identification of novel human and rodent CB2 isoforms, differential tissue expression and regulation by cannabinoid receptor ligands. *Genes Brain Behav.* **2009**, *8*, 519–530. [[CrossRef](#)]
49. Li, Y.; Li, C.; Li, S.; Peng, Q.; An, N.A.; He, A.; Li, C.Y. Human exonization through differential nucleosome occupancy. *Proc. Natl. Acad. Sci. USA* **2018**, *115*, 8817–8822. [[CrossRef](#)]
50. Fan, L.; Westermark, G.; Chan, S.J.; Steiner, D.F. Altered gene structure and tissue expression of islet amyloid polypeptide in the chicken. *Mol. Endocrinol.* **1994**, *8*, 713–721.
51. Toshimori, H.; Narita, R.; Nakazato, M.; Asai, J.; Mitsukawa, T.; Kangawa, K.; Matsuo, H.; Matsukura, S. Islet amyloid polypeptide (IAPP) in the gastrointestinal tract and pancreas of man and rat. *Cell Tissue Res.* **1990**, *262*, 401–406. [[CrossRef](#)] [[PubMed](#)]
52. Dupin, M.; Fortin, T.; Larue-Triolet, A.; Surault, I.; Beaulieu, C.; Gouel-Cheron, A.; Allaouchiche, B.; Asehnoune, K.; Roquilly, A.; Venet, F.; et al. Impact of Serum and Plasma Matrices on the Titration of Human Inflammatory Biomarkers Using Analytically Validated SRM Assays. *J. Proteome Res.* **2016**, *15*, 2366–2378. [[CrossRef](#)]
53. Guzel, C.; Govorukhina, N.I.; Stingl, C.; Dekker, L.J.M.; Boichenko, A.; van der Zee, A.G.J.; Bischoff, R.P.H.; Luider, T.M. Comparison of Targeted Mass Spectrometry Techniques with an Immunoassay: A Case Study for HSP90alpha. *Proteom. Clin. Appl.* **2018**, *12*, 1700107. [[CrossRef](#)]
54. El Haj, M.; Antoine, P.; Amouyel, P.; Lambert, J.C.; Pasquier, F.; Kapogiannis, D. Apolipoprotein E (APOE) epsilon4 and episodic memory decline in Alzheimer's disease: A review. *Ageing Res. Rev.* **2016**, *27*, 15–22. [[CrossRef](#)] [[PubMed](#)]

55. Hanlon, C.S.; Rubinsztein, D.C. Arginine residues at codons 112 and 158 in the apolipoprotein E gene correspond to the ancestral state in humans. *Atherosclerosis* **1995**, *112*, 85–90. [[CrossRef](#)] [[PubMed](#)]
56. McIntosh, A.M.; Bennett, C.; Dickson, D.; Anestis, S.F.; Watts, D.P.; Webster, T.H.; Fontenot, M.B.; Bradley, B.J. The apolipoprotein E (APOE) gene appears functionally monomorphic in chimpanzees (*Pan troglodytes*). *PLoS ONE* **2012**, *7*, e47760. [[CrossRef](#)]
57. De Franco, E.; Owens, N.D.L.; Montaser, H.; Wakeling, M.N.; SaarimäkiVire, J.; Ibrahim, H.; Triantou, A.; Balboa, D.; Caswell, R.C.; Johnson, M.B.; et al. Primate-Specific ZNF808 Is Essential for Pancreatic Development in Humans. 2021. Available online: <https://www.medrxiv.org/content/10.1101/2021.08.23.21262262v1> (accessed on 10 November 2022).
58. Ding, Y.; Luan, W.; Shen, X.; Wang, Z.; Cao, Y. LncRNA BDNF-AS as ceRNA regulates the miR-9-5p/BACE1 pathway affecting neurotoxicity in Alzheimer's disease. *Arch. Gerontol. Geriatr.* **2022**, *99*, 104614. [[CrossRef](#)]
59. Wang, S.; Fan, Y.; Xu, Y.; Zhang, L.; Cai, L.; Lv, B. GDNFOS1 knockdown decreases the invasion and viability of glioblastoma cells. *Exp. Ther. Med.* **2019**, *18*, 1315–1322. [[CrossRef](#)] [[PubMed](#)]
60. Li, C.Y.; Zhang, Y.; Wang, Z.; Zhang, Y.; Cao, C.; Zhang, P.W.; Lu, S.J.; Li, X.M.; Yu, Q.; Zheng, X.; et al. A human-specific de novo protein-coding gene associated with human brain functions. *PLoS Comput. Biol.* **2010**, *6*, e1000734. [[CrossRef](#)]
61. Yang, Y.; Xie, B.; Ju, C.; Jin, H.; Ye, X.; Yao, L.; Jia, M.; Sun, Z.; Yuan, Y. The Association of Decreased Serum Gdnf Level with Hyperglycemia and Depression in Type 2 Diabetes Mellitus. *Endocr. Pract.* **2019**, *25*, 951–965. [[CrossRef](#)]
62. Saini, R.K.; Goyal, D.; Goyal, B. Targeting Human Islet Amyloid Polypeptide Aggregation and Toxicity in Type 2 Diabetes: An Overview of Peptide-Based Inhibitors. *Chem. Res. Toxicol.* **2020**, *33*, 2719–2738. [[CrossRef](#)] [[PubMed](#)]
63. Hishimoto, A.; Pletnikova, O.; Lang, D.L.; Troncoso, J.C.; Egan, J.M.; Liu, Q.R. Neurexin 3 transmembrane and soluble isoform expression and splicing haplotype are associated with neuron inflammasome and Alzheimer's disease. *Alzheimers Res. Ther.* **2019**, *11*, 28. [[CrossRef](#)] [[PubMed](#)]
64. De Meyer, S.; Schaefferbeke, J.M.; Verberk, I.M.W.; Gille, B.; De Schaeppdryver, M.; Luckett, E.S.; Gabel, S.; Bruffaerts, R.; Mauroo, K.; Thijssen, E.H.; et al. Comparison of ELISA- and SIMOA-based quantification of plasma Aβ ratios for early detection of cerebral amyloidosis. *Alzheimers Res. Ther.* **2020**, *12*, 162. [[CrossRef](#)]
65. Meng, X.; Li, T.; Wang, X.; Lv, X.; Sun, Z.; Zhang, J.; Su, F.; Kang, S.; Kim, S.; An, S.S.A.; et al. Association between increased levels of amyloid-beta oligomers in plasma and episodic memory loss in Alzheimer's disease. *Alzheimers Res. Ther.* **2019**, *11*, 89. [[CrossRef](#)] [[PubMed](#)]
66. Thijssen, E.H.; La Joie, R.; Strom, A.; Fonseca, C.; Iaccarino, L.; Wolf, A.; Spina, S.; Allen, I.E.; Cobigo, Y.; Heuer, H.; et al. Plasma phosphorylated tau 217 and phosphorylated tau 181 as biomarkers in Alzheimer's disease and frontotemporal lobar degeneration: A retrospective diagnostic performance study. *Lancet Neurol.* **2021**, *20*, 739–752. [[CrossRef](#)] [[PubMed](#)]
67. Chen, Z.; Mengel, D.; Keshavan, A.; Rissman, R.A.; Billinton, A.; Perkinson, M.; Percival-Alwyn, J.; Schultz, A.; Properzi, M.; Johnson, K.; et al. Learnings about the complexity of extracellular tau aid development of a blood-based screen for Alzheimer's disease. *Alzheimers Dement.* **2019**, *15*, 487–496. [[CrossRef](#)] [[PubMed](#)]
68. Mattsson, N.; Andreasson, U.; Zetterberg, H.; Blennow, K.; Alzheimer's Disease Neuroimaging, I. Association of Plasma Neurofilament Light With Neurodegeneration in Patients With Alzheimer Disease. *JAMA Neurol.* **2017**, *74*, 557–566. [[CrossRef](#)] [[PubMed](#)]
69. Kapogiannis, D.; Mustapic, M.; Shardell, M.D.; Berkowitz, S.T.; Diehl, T.C.; Spangler, R.D.; Tran, J.; Lazaropoulos, M.P.; Chawla, S.; Gulyani, S.; et al. Association of Extracellular Vesicle Biomarkers with Alzheimer Disease in the Baltimore Longitudinal Study of Aging. *JAMA Neurol.* **2019**, *76*, 1340–1351. [[CrossRef](#)]
70. Ashton, N.J.; Leuzy, A.; Karikari, T.K.; Mattsson-Carlsson, N.; Dodich, A.; Boccardi, M.; Corre, J.; Drzezga, A.; Nordberg, A.; Ossenkoppele, R.; et al. The validation status of blood biomarkers of amyloid and phospho-tau assessed with the 5-phase development framework for AD biomarkers. *Eur. J. Nucl. Med. Mol. Imaging* **2021**, *48*, 2140–2156. [[CrossRef](#)]

**Disclaimer/Publisher's Note:** The statements, opinions and data contained in all publications are solely those of the individual author(s) and contributor(s) and not of MDPI and/or the editor(s). MDPI and/or the editor(s) disclaim responsibility for any injury to people or property resulting from any ideas, methods, instructions or products referred to in the content.